ARTICLE

Activation of 4-1BBL^{+} B cells with CD40 agonism and IFNγ elicits potent immunity against glioblastoma

Catalina Lee-Chang[1], Jason Miska[1], David Hou[1], Aida Rashidi[1], Peng Zhang[1], Rachel A. Burga[1], Ignacio Jusué-Torres[1,2], Ting Xiao[1], Victor A. Arrieta[1,3], Daniel Y. Zhang[1], Aurora Lopez-Rosas[1], Yu Han[1], Adam M. Sonabend[1], Craig M. Horbinski[1,4], Roger Stupp[1,5], Irina V. Balyasnikova[1], and Maciej S. Lesniak[1]

Immunotherapy has revolutionized the treatment of many tumors. However, most glioblastoma (GBM) patients have not, so far, benefited from such successes. With the goal of exploring ways to boost anti-GBM immunity, we developed a B cell–based vaccine (B$_{Vax}$) that consists of 4-1BBL^{+} B cells activated with CD40 agonism and IFNγ stimulation. B$_{Vax}$ migrates to key secondary lymphoid organs and is proficient at antigen cross-presentation, which promotes both the survival and the functionality of CD8^{+} T cells. A combination of radiation, B$_{Vax}$, and PD-L1 blockade conferred tumor eradication in 80% of treated tumor-bearing animals. This treatment elicited immunological memory that prevented the growth of new tumors upon subsequent reinjection in cured mice. GBM patient–derived B$_{Vax}$ was successful in activating autologous CD8^{+} T cells; these T cells showed a strong ability to kill autologous glioma cells. Our study provides an efficient alternative to current immunotherapeutic approaches that can be readily translated to the clinic.

Introduction

Despite the tremendous effort in basic, translational, and clinical research, the standard of care (SoC) of patients with glioblastoma (GBM) has been virtually unchanged for the past two decades (Stupp et al., 2017), aside from tumor-treating fields (Taphoorn et al., 2018). GBM is one of the immunologically "coldest tumors" in which T cell exclusion is at its maximum, and myeloid infiltration predominates (Thorsson et al., 2018). This is due to profound immunosuppression (Raychaudhuri et al., 2011; Wintterle et al., 2003), the metabolically hostile microenvironment (Li et al., 2009), and the low mutational burden of these tumors (Iranzo et al., 2018). Together, these barriers have hindered the development of effective immunotherapies (Vega et al., 2008; Wainwright et al., 2012b).

The first immunotherapies tested in the clinic used dendritic cell (DC)–based vaccines as a way to promote endogenous immunity against GBM (Eagles et al., 2018; Prins et al., 2013; Wen et al., 2019). In many of these trials, DCs were pulsed with autologous tumor lysate, while others injected immunogenic epitopes against tumor-associated antigens (Ags; Weller et al., 2017). To date, these approaches have only met with limited success, although many more trials are still underway (Eagles et al., 2018). Several emerging therapeutic strategies, such as

checkpoint blockade (Maxwell et al., 2017) or adoptive transfer of chimeric Ag-receptor T cells targeting GBM-Ags, are also being explored (Pituch et al., 2018). However, their effectiveness remains to be determined. While immunotherapy remains an attractive approach for GBM patients, we have yet to significantly promote antitumor immunity in these patients to achieve a clinical benefit.

The B cell–based vaccine is a promising yet underinvestigated approach to boost anticancer immunity (Kim et al., 2014; Schultze et al., 1997). There are three main advantages of B cells as cellular-based vaccines: (1) they can be readily manufactured ex vivo; (2) they can share cognate Ag specificity with T cells (Wennhold et al., 2017); and (3) they have high mobility, which allows their homing to key secondary lymphoid organs (SLOs) as well as tumors (Gonzalez et al., 2015).

However, a key reason why B cell antitumor vaccines have not garnered more interest is that B cells can quickly switch between anti- and protumorigenic phenotypes within the surrounding microenvironment. For example, B cells become immunosuppressive within GBM and represent ~10% of infiltrating immune cells (Lee-Chang et al., 2019). Yet tumor-infiltrating B cells do show an antitumor effect in a variety of

[1]Department of Neurological Surgery, Feinberg School of Medicine, Northwestern University, Chicago, IL; [2]Department of Neurological Surgery, Loyola University Chicago Stritch School of Medicine, Chicago, IL; [3]Plan de Estudios Combinados en Medicina, National Autonomous University of Mexico, Mexico City, Mexico; [4]Department of Pathology, Feinberg School of Medicine, Northwestern University, Chicago, IL; [5]Division of Hematology/Oncology, Feinberg School of Medicine, Northwestern University, Chicago, IL.

Correspondence to Catalina Lee-Chang: catalina.leechang@northwestern.edu; Maciej S. Lesniak: maciej.lesniak@northwestern.edu.

cancers (Tsou et al., 2016). Their function has been linked to the production of antitumor antibodies (Abs; Garaud et al., 2019) and their APC function and activation of effector T cells (Bruno et al., 2017; Nielsen et al., 2012), so there is still potential for B cell–based antitumor therapies.

Studies on B cell–driven inflammation have identified a subset of B cells expressing the costimulatory marker 4-1BBL (or CD137L) capable of enhancing CD8^{+} T cell antitumor cytotoxicity. Such activation was achieved through multiple mechanisms, including Ag presentation, T cell costimulation (4-1BBL and CD86), and cytokine production (TNFα; Lee-Chang et al., 2016, 2014). Thus, 4-1BBL^{+} B cells could be used to boost antitumor CD8^{+} T cell response. To stabilize their Ag presentation function in vivo and avoid potential immunosuppressive functions, we activated 4-1BBL^{+} B cells using CD40 and IFNγ receptor (IFNγR) ligation (designated as B_{Vax}), both of which were known to effectively enhance B cell–mediated Ag presentation (Ahmadi et al., 2008; Braun et al., 2002; Lapointe et al., 2003).

In the present study, we explored the ability of B_{Vax} to inhibit GBM growth by promoting tumor-specific CD8^{+} T cell immunity. B_{Vax}'s therapeutic effectiveness was examined both alone and in combination with radiation and checkpoint blockade.

Results

Functional status of 4-1BBL–expressing B cells
In GBM patients' peripheral blood, 4-1BBL^{+} B cells represented 13.75% ± 2.3% of total CD20^{+} CD19^{+} B cell compartment (peripheral blood mononuclear cells [PBMCs]; $n = 90$; Fig. 1 A and Table 1). These 4-1BBL^{+} B cells show increased levels of intracellular TNFα and IFNγ, as well as expression of activation marker CD86 and CD69 expression levels (Fig. 1 B) compared with 4-1BBL^{−} B cells, suggestive of their activated status. The relative abundance of 4-1BBL^{+} B cells was associated with increased numbers of activated CD69^{+}CD8^{+} T cells (Fig. 1 C), suggestive of a systemic activated immune-profile of the patients. Accordingly, GBM patient–derived 4-1BBL^{+} B cells showed greater ability to enhance CD8^{+} T cell costimulation in the presence of exogenous TCR stimulation (anti-CD3) compared with 4-1BBL^{−} B cells, as shown by increased cell proliferation (measured as expansion index; Fig. 1 D) and expansion of effector IFNγ and granzyme B (GzmB)–expressing cells (Fig. 1 E). In the preclinical CT2A glioma mouse model, 4-1BBL expression on B cells was not detected in tumor-bearing brains. Its expression was significantly higher in B cells from both deep and superficial cervical LNs (CLNs) after tumor inoculation, suggesting a tumor-mediated induction of 4-1BBL expression by B cells (Fig. S1 A). The ability of B cells to costimulate CD8^{+} T cells largely depended on the expression of 4-1BBL. 4-1BBL upregulation in B cells is driven after B cell receptor (BCR) stimulation and CD40 cognate help (Futagawa et al., 2002). In support of these observations, BCR- and CD40-stimulated B cells in the presence of B cell–activating factor of the TNF family (BAFF) could promote the proliferation of effector CD8^{+} T cells (Fig. S1 B). This function required the ability of these B cells to express 4-1BBL, as its absence dampened the CD8^{+} T cell activation

function (Fig. S1 B). Overall, these data suggest that 4-1BBL^{+} B cells are activated cells, capable of expanding and promoting the CD8^{+} T cell effector phenotype.

CD40 and IFNγR stimulation potentiates the APC phenotype and function of 4-1BBL^{+} B cells
CD40 ligation is a well-studied process that leads to B cell activation, proliferation, and enhancement of Ag-presenting and costimulatory functions (Fig. S1 B; Ahmadi et al., 2008; Lapointe et al., 2003). However, it has also been associated with the generation of immunosuppressive and regulatory B cells in different inflammatory and autoimmune conditions (Yoshizaki et al., 2012). To generate stable APC B cells, we tested the activation of the IFNγR, as it can drive B cell costimulatory molecule expression (Braun et al., 2002). We observed that IFNγ caused up-regulation of CD86 expression on unstimulated human B cells (Fig. S2 A), a key costimulatory molecule in CD8^{+} T cell activation (Lee-Chang et al., 2014). The pro-activating effect of IFNγ was proven by the utilization of B cells deficient in IFNγR (Fig. S2 B). However, IFNγ alone could not promote B cells able to activate CD8^{+} T cells in the presence of TCR stimulation (anti-CD3; Fig. S1 B), suggesting that IFNγR stimulation could potentiate rather than initiate B cell–mediated CD8^{+} T cell costimulation. Also, we observed that both CD40 and IFNγR stimulation additively up-regulated CD86 (Fig. S2 B), suggesting that dual activation can further promote the APC-like phenotype of B cells.

Based on these results, CD40 agonism and IFNγ were used to activate in vitro 4-1BBL^{+} B cells isolated from glioma-bearing mice's SLOs, such as deep and superficial CLNs and spleens (Fig. S2 C). BAFF was used to enhance B cell survival. After a total of 48 h of culture, cells were harvested and evaluated for the expression of APC markers. Compared with 4-1BBL^{−} B cells incubated with only BAFF (designated as B_{Naive}), activated 4-1BBL^{+} B cells (designated as B_{Vax}) showed up-regulation of both MHC-classes I (H-2K[b]) and II (IA[b]) on their surface (Fig. S2, C and D). After the cells were pulsed with the OVA peptide SIINFEKL, B_{Vax} highly coexpressed SIINFEKL–H-2K[b] complex and costimulatory markers CD86 and 4-1BBL (Fig. 1 F).

Professional APCs are known for their ability to cross-present exogenous Ags to CD8^{+} T cells via MHC class I (Fu and Jiang, 2018). To evaluate whether B_{Vax} can cross-present, they were incubated with a fluorescently conjugated OVA protein (Alexa Fluor 488-OVA; Fig. 1 G). OVA protein uptake was visualized using epifluorescent microscopy (Fig. 1 G). After 3 h, we observed B_{Vax} had substantial levels of surface H-2K[b]–SIINFEKL complex, as observed by flow cytometric analysis, while B_{Vax} treated with Golgi transporter inhibitor brefeldin A did not (Fig. 1 H). Next, we evaluated the ability of OVA–pulsed B_{Vax} to activate SIINFEKL-specific OT-I CD8^{+} T cells. We included bone marrow–derived DCs as a gold standard of professional APC able to cross-present. B_{Naive}, B_{Vax}, and DCs pulsed with SIINFEKL peptide induced the proliferation of OT-I CD8^{+} T cells, as well as their up-regulation of GzmB (Fig. S2 E). This phenomenon was dependent on TCR ligation, as unpulsed cells (no Ag) failed to activate OT-I CD8^{+} T cells (Fig. S2 E) and SIINFEKL-pulsed APCs could not activate CD8^{+} T cells from WT C57BL/6 mice (Fig. S2 F). However, when B cells and DCs were pulsed with OVA
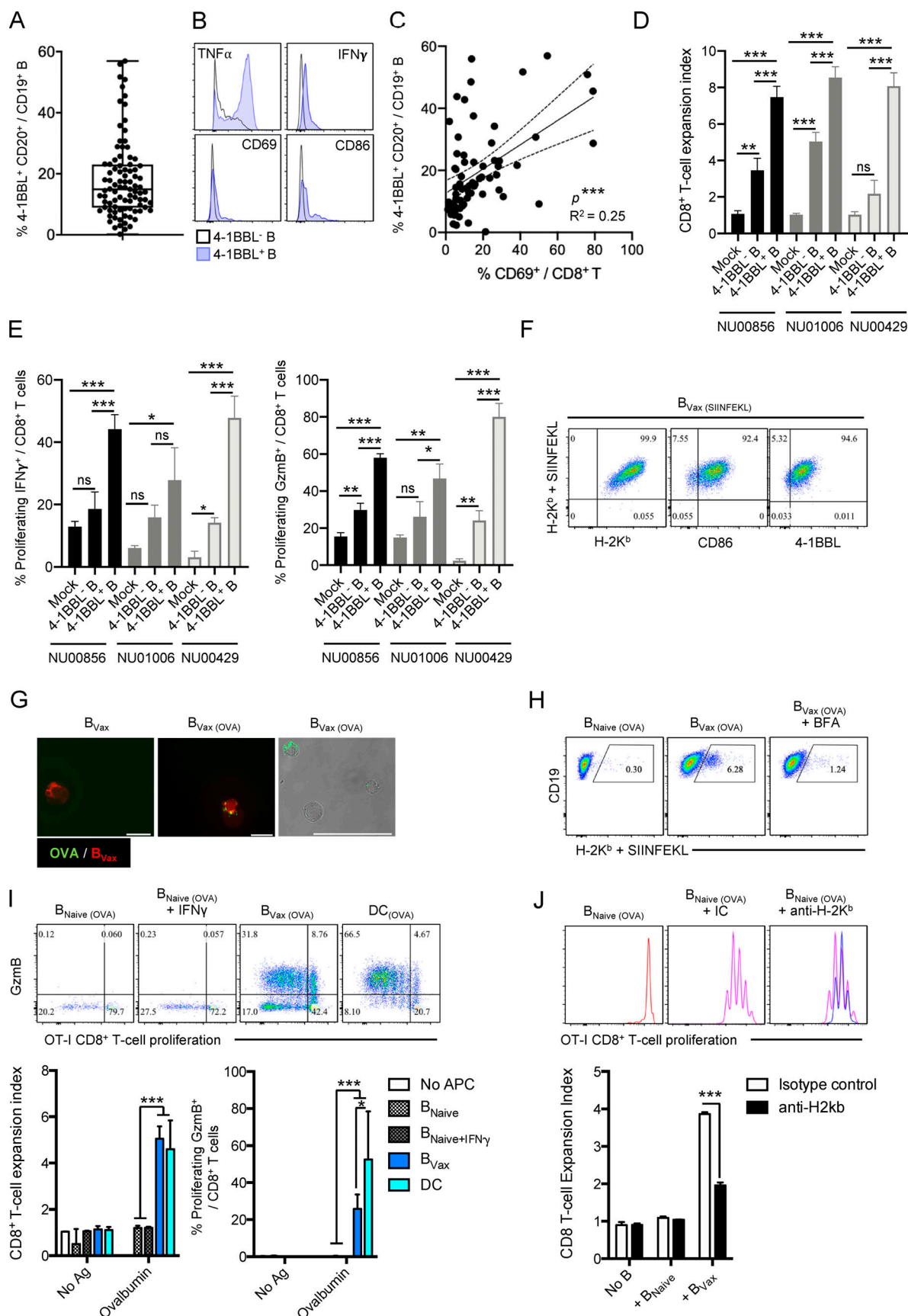
Figure 1. 4-1BBL⁺ B cells in GBM patients' peripheral blood and Ag-presenting function. (A) Box plot showing the expression of 4-1BBL in CD20⁺CD19⁺ B cells from newly diagnosed GBM patients' PBMCs ($n = 90$). Box plots express the following values: median (line inside the box), 75th and 25th percentiles (box

extremities), and maximum and minimum values (dashes). **(B)** Histograms representing the intracellular expression of TNFα and IFNγ and surface expression of CD69 and CD86 by 4-1BBL⁻ (black line) and 4-1BBL⁺ (blue line) B cells. **(C)** Linear regression analysis of 4-1BBL expression by B cells and CD69 expression by CD8⁺ T cells in newly diagnosed GBM patients' PBMCs ($n = 68$). **(D and E)** CD8⁺ T cell costimulation assay using CD8⁺ T cells activated with anti-CD3 and IL-2 mixed with autologous 4-1BBL⁻ and 4-1BBL⁺ B cells from peripheral blood of three newly diagnosed GBM patients (NU00856, NU01006, and NU00429). CD8⁺ T cell activation was measured as cellular expansion (D) and expression of intracellular IFNγ and GzmB (E). The experiment was performed in triplicate. **(F)** B_{Vax} from GL261-OVA mice were pulsed with SIINFEKL ($B_{Vax(SIINFEKL)}$) and evaluated for SIINFEKL presentation by MHC class I (H-2Kᵇ + SIINFEKL Ab) and the coexpression of MHC class I (H-2Kᵇ) and costimulatory molecules CD86 and 4-1BBL. A representative experiment of three independent experiments is shown. **(G and H)** B_{Vax} were tested for their ability to uptake Alexa Fluor 488–conjugated OVA ($B_{Vax[OVA]}$; G) and present SIINFEKL peptide via MHC class I (H-2Kᵇ; H). Surface transport of the H-2Kᵇ + SIINFEKL complex was inhibited using brefeldin A (BFA). A representative experiment of three independent experiments is shown. Scale bars represent 15 μm (fluorescence images) and 50 μm (fluorescence and bright light image). **(I)** B_{Naive}, B_{Naive} + IFNγ, B_{Vax}, and DCs were pulsed with OVA and tested for their ability to promote OT-I CD8⁺ T cell activation assessed by cell proliferation (expansion index, x axis) and intracellular expression of GzmB (y axis). The experiment was performed in triplicate. A representative experiment of two independent experiments is shown. **(J)** OT-I CD8⁺ T cells cultured with B_{Naive}; B_{Vax} pulsed with OVA and isotype control, $B_{Vax(OVA)}$ + IC; or MHC class I blocking Ab, $B_{Vax(OVA)}$ + anti-H2Kᵇ, and tested for their cellular expansion. A representative experiment of two independent experiments is shown. Differences among multiple groups were evaluated using one-way ANOVA with post hoc Tukey's multiple comparisons test. Statistical significance is depicted as follows: *, $P < 0.05$; **, $P < 0.01$; ***, $P < 0.001$. ns, not statistically significant.

protein, only B_{Vax} and DCs were able to successfully activate OT-I CD8⁺ T cells (Fig. 1 I). Blockade of MHC class I abrogated the APC function of B_{Vax} (Fig. 1 J). Altogether, these data suggest that B_{Vax} has the adequate constellation of surface molecules to promote CD8⁺ T cell activation and can cross-present Ags via MHC class I as a professional APC in vitro.

Table 1. **Baseline characteristics of newly diagnosed GBM patients**

Patient characteristics	n = 90
Age at diagnosis, yr (IQR)	64 (55–70)
Gender	
Male (%)	47 (52)
Female (%)	43 (48)
Race	
White (%)	75 (97)
Black (%)	2 (3)
Ethnicity	
Hispanic (%)	75 (97)
Non-Hispanic (%)	2 (3)
IDH-1 status	
WT (%)	84 (93)
Mutated (%)	6 (7)
MGMT promoter	
Unmethylated (%)	53 (59)
Methylated (%)	34 (38)
P53 stain, % (IQR)	5 (2–20%)
Ki67, % (IQR)	30 (16–40%)
Preoperative steroid use, n (%)	85 (94)
Median overall survival, mo (95% confidence interval)	15 (12–19)
1-yr survival, n at risk (survival probability)	37 (59%)
2-yr survival, n at risk (survival probability)	12 (26%)

IDH, isocitrate dehydrogenase; IQR, interquartile range; MGMT, O[6]-methylguanine-DNA.

B_{Vax} are potent APCs in vivo

Next, we aimed to test the APC function of B_{Vax} in vivo. First, C57BL/6 mice were intracranially injected with GL261 overexpressing the OVA protein (GL261-OVA). These mice were used as B_{Vax} and CD8⁺ T cell donors. B_{Vax} were pulsed with OVA, and CD8⁺ T cells were fluorescently labeled using the eFluor450 dye and concomitantly injected i.v. into Rag1-deficient mice bearing the GL261-OVA tumor. Administration of B_{Vax} increased the numbers of eFluor450⁺ CD8⁺ T cells in tumor-bearing brains and deep cervical lymph nodes (dCLNs) compared with B_{Naive} or untreated Mock groups (Fig. 2 A). Next, B cell–deficient (B KO) mice bearing GL261-OVA received OVA–pulsed B_{Vax}. Treated mice showed a substantial increase of endogenous SIINFEKL-specific CD8⁺ T cells infiltrating the tumor-bearing brains (Fig. 2 B and Fig. S2 G). A group of mice that received B_{Vax} pretreated in vitro with the pertussis toxin (PTX), which inhibits G protein–mediated cellular migration (Cyster and Goodnow, 1995), did not induce SIINFEKL-specific CD8⁺ T cells as well (Fig. 2 B). In the CT2A glioma model, B_{Vax} pulsed with CT2A–tumor lysates ($B_{Vax(CT2A)}$) increased the number of activated GzmB- and IFNγ-producing CD8⁺ T cells in the tumor-bearing brains (Fig. 2 C). The loss of CD8⁺ T cell activation in mice receiving $B_{Vax(CT2A)}$ + PTX highlights the importance of tissue recruitment of B_{Vax}. Accordingly, B_{Vax} colocalized with CD8⁺ T cells in SLOs such as spleens and CLNs after concomitant i.v. injection (Fig. 2 D). In addition, while B_{Vax} (and B_{Naive}) were detected in the draining dCLNs and the circulation, only B_{Vax} were found in the tumor-bearing brains (Fig. S3 A).

As we recently reported that myeloid-derived suppressive cells could generate regulatory B cells within the tumor vicinity (Lee-Chang et al., 2019), we next determined whether tumor-infiltrating B_{Vax} could be converted into immunosuppressive B cells. Our data showed that tumor-infiltrating B_{Naive} and B_{Vax} differ in their ability to promote CD8⁺ T cell activation. After intracranial injection, B_{Vax} maintained their CD8⁺ T cell activating function, whereas injection of B_{Naive} resulted in T cell inhibition (Fig. S3 B; after injection). Altogether, our results confirm that B_{Vax} are resistant to tumor immunosuppression and maintained their T cell activating function in vivo. In support of this, B_{Vax} therapy extended CT2A-bearing animal survival compared with mice treated with B_{Naive} or activated with
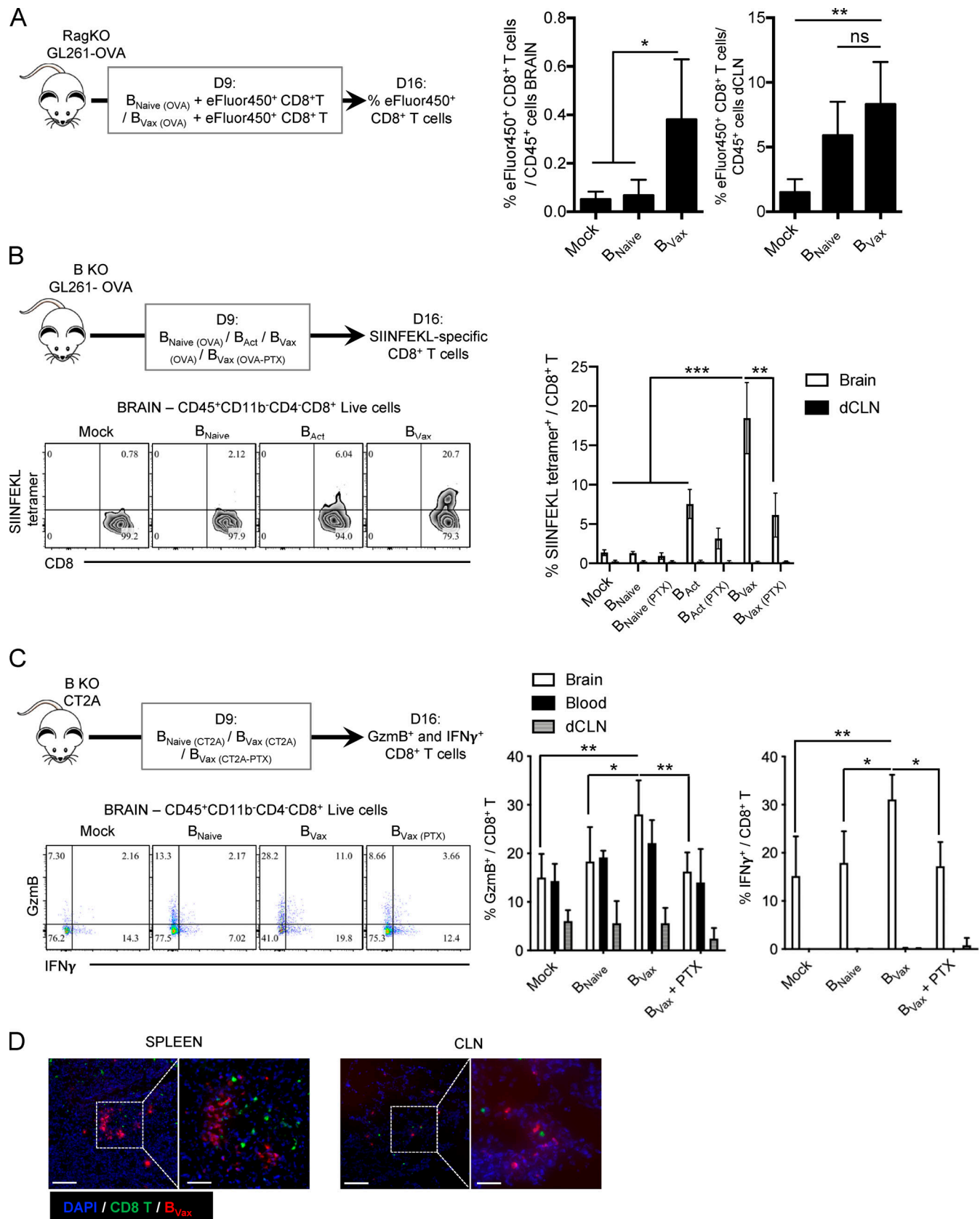
Figure 2. **B_Vax APC function in vivo. (A)** Rag1-deficient mice were challenged intracranially with GL261-OVA. 9 d after, mice received i.v. B_Naive or B_Vax pulsed with OVA protein. eFluor450-labeled CD8+ T cells from WT C57BL/6 mice were concomitantly injected with B cells (n = 4 mice/group). 7 d after the cell adoptive transfer, eFluor450+ CD8+ T cells were evaluated by flow cytometry in the tumor-bearing brains and the dCLNs. A representative experiment of two

independent experiments is shown. **(B)** B KO mice were challenged intracranially with GL261-OVA. 9 d after, mice received i.v. B$_{Naive}$, 4-1BBL$^-$ B cells activated with CD40 agonism and IFNγ (B$_{Act}$) or B$_{Vax}$ pulsed with OVA protein. A group of B$_{Vax(OVA)}$ mice was pretreated with PTX before injection (n = 4 mice/group). 7 d after the cell adoptive transfer, SIINFEKL-specific CD8$^+$ T cells were analyzed in the tumor-bearing brains by flow cytometry using SIINFEKL-tetramer. A representative experiment of two independent experiments is shown. **(C)** B KO mice were challenged intracranially with CT2A cells. 9 d after, mice received i.v. B$_{Naive}$ and B$_{Vax}$ pulsed with CT2A tumor lysates pretreated with or without PTX (n = 5 mice/group). 7 d after the cell adoptive transfer, CD8$^+$ T cells were evaluated for the intracellular expression of GzmB and IFNγ in the tumor-bearing brain, blood, and dCLNs. A representative experiment of three independent experiments is shown. **(D)** Rag1-deficient (KO) mice were challenged intracranially with CT2A cells. 9 d after, mice i.v. and concomitantly received both CellTracker red CMPTX B$_{Vax}$ (red) cells and CellTracker green CMFDA-labeled CD8$^+$ T cells (green). B$_{Vax}$ and CD8$^+$ T cell splenic localization was analyzed by fluorescent microscopy. Scale bars represent 100 μm (left image, 20× magnification) and 50 μm (right image, 63× magnification). Images are representative of the spleen and CLN of three mice. For all experiments shown in this figure, differences among multiple groups were evaluated using one-way ANOVA with post hoc Tukey's multiple comparisons test. Histograms are shown as mean ± SD. Statistical significance is depicted as follows: *, P < 0.05; **, P < 0.01; ***, P < 0.001. ns, not statistically significant.

CD40 agonist and IFNγ B cells but 4-1BBL$^-$ (B$_{Act}$; Mock median survival: 24 d; B$_{Naive}$: 17.5; B$_{Act}$: 18; and B$_{Vax}$: 34; Mock versus B$_{Vax}$: P = 0.006; Fig. S3 C). B$_{Vax}$ therapeutic effect was abrogated when 4-1BBL blocking Ab was used (Mock median survival: 23.5 d; B$_{Vax}$: 35.5; B$_{Vax}$ + anti–4-1BBL: 22.5; and B$_{Vax}$: 34; B$_{Vax}$ versus B$_{Vax}$ + anti–4-1BBL: P = 0.0016; Fig. S3 D), suggesting the key role of this molecule in B$_{Vax}$-mediated immune functions.

Radiotherapy promotes B$_{Vax}$ expansion and persistence in the SLOs

It has been reported that, in GBM patients, radiation and temozolomide (TMZ) treatment increases the systemic production of BAFF, a key factor for the survival of B cells (Sanchez-Perez et al., 2013; Saraswathula et al., 2016). This suggests that current treatment might provide an adequate environment for the in vivo adaptation of B cells. To test this hypothesis, CT2A-bearing mice received a lymphodepleting dose of irradiation (whole-body radiotherapy [RTx]; Fig. S4 A). Then, mice received B$_{Vax}$ obtained from CD45.1$^+$ congenic mice. After 5 d, we observed that CD45.1$^+$ B$_{Vax}$ counts were increased in mice treated with RTx compared with the untreated Mock group (Fig. 3 A). Serum BAFF levels were significantly higher in the RTx group and were sustained over the duration of the experiment (5 d; Fig. 3 B). Since BAFF levels were lower in tumor-bearing mice than in tumor-free mice, this suggests that the tumor might disrupt the B cell homeostatic balance and drive the drastic B cell depletion observed in the peripheral compartment (Lee-Chang et al., 2019). As BAFF is a survival factor for any B cell subtype (Mackay and Browning, 2002), we performed the same adoptive transfer of CD45.1$^+$ B cells but used different B cell subsets, such as B$_{Naive}$, activated with CD40 agonist and IFNγ B cells but 4-1BBL$^-$ (B$_{Act}$) and B$_{Vax}$. All B cell subtypes were found in the spleen; however, more B$_{Vax}$ were obtained in the dCLNs (Fig. 3 C), known to drain the central nervous system (CNS; Louveau et al., 2018). The majority of dCLN-homing B$_{Vax}$ were in a proliferative cellular state, as shown by the expression of Ki67 (Fig. 3 C). Pretreatment of B cells and systemic injection with BAFF receptor (BAFF-R)–blocking Ab reduced the B$_{Vax}$ counts in vivo (Fig. 3 D), suggesting that BAFF secretion upon RTx controls B$_{Vax}$ in vivo adaptation.

Next, B$_{Vax}$ therapeutic effect was tested in vivo in mice treated with or without RTx. CT2A-bearing mice were treated with RTx 7 d after tumor implantation, and B$_{Vax}$ pulsed with CT2A tumor lysates were i.v. injected 2 d after RTx, after tumor

engraftment and significant tumor mass were confirmed by histology (Fig. S4 B). B$_{Vax}$ pulsed with tumor lysates provided slight but significantly extended animal survival in combination with RTx (Mock median survival: 17 d; RTx: 18; B$_{Vax}$: 22; and B$_{Vax}$ + RTx: 28; B$_{Vax}$ versus B$_{Vax}$ + RTx: P < 0.0001; Fig. S3 C).

As RTx induced general lymphopenia (Fig. S4 C), we postulated that the lack of B$_{Vax}$ target cells (CD8$^+$ T cells) would limit the therapeutic effectiveness of the vaccine. Thus, we administered B$_{Vax}$ (pulsed with tumor lysates) concomitantly with CD8$^+$ T cells obtained from CT2A glioma–bearing mice. Mice that received RTx and a single shot of B$_{Vax}$ showed improved overall survival (Mock versus B$_{Vax}$: P = 0.0001). However, mice that received both B$_{Vax}$ and CD8$^+$ T cells survived longer than all other groups (Mock median survival: 16 d; CD8$^+$ T: 19 d; B$_{Vax}$: 27.5 d; B$_{Vax}$ + CD8$^+$ T: 35 d; B$_{Vax}$ versus B$_{Vax}$ + CD8$^+$ T: P = 0.0001; Fig. 3 E). Similar results, although modest, were obtained in mice treated with B$_{Vax}$ and CD8$^+$ T cells at late stages of tumor progression (9 d versus 15 d after tumor implantation [D9 or D15]; Mock median survival: 20 d; B$_{Vax}$ [D9]: 26; B$_{Vax}$ + CD8$^+$ T [D9]: 35; B$_{Vax}$ [D15]: 19; B$_{Vax}$ + CD8$^+$ T [D15]: 25; B$_{Vax}$ + CD8$^+$ T [D9] versus B$_{Vax}$ + CD8$^+$ T [D15]: P = 0.0003; Fig. S4, B and D). A single shot of B$_{Vax}$ (pulsed with tumor lysate) + CD8$^+$ T cell combination provided improved therapeutic benefit compared with DC (pulsed with tumor lysates), which was administered either i.v. or intradermally (i.d.; Mock median survival: 16 d; CD8$^+$ T: 22; DC$_{(i.d.)}$ + CD8$^+$ T: 16; DC$_{(i.v.)}$ + CD8$^+$ T: 20; B$_{Vax(i.v.)}$ + CD8$^+$ T: 34; DC$_{(i.v.)}$ + CD8$^+$ T versus B$_{Vax(i.v.)}$ + CD8$^+$ T: P = 0.0029; Fig. 3 F).

To test whether in vivo persistence of these different cellular-based therapies was associated with different outcomes, B$_{Vax}$ and DCs were fluorescently labeled with the cell proliferation dye eFluor450 and administered to RT-treated CT2A-bearing mice. 5 d after the adoptive transfer, eFluor450$^+$ cells were quantified. Accumulation of B$_{Vax}$ was significantly higher than that of DCs. By examining the dilution of the eFluor450 dye, we observed that B$_{Vax}$ had a high proliferative phenotype (Fig. 3 G).

Also, we performed in vivo imaging tracking of CD8$^+$ T cells labeled with far-red fluorescence coinjected with either B$_{Vax}$ or DC (both pulsed with CT2A tumor lysates). CD8$^+$ T cell accumulation in the CT2A-bearing brains was enhanced when cells were administered concomitantly with B$_{Vax}$ 30 h after injection (Fig. 4 A). The decrease in the signal at later time points could be due to the limited display of dye fluorescence. Thus, in a parallel experiment, mice received CD45.1$^+$CD8$^+$ T cells together with
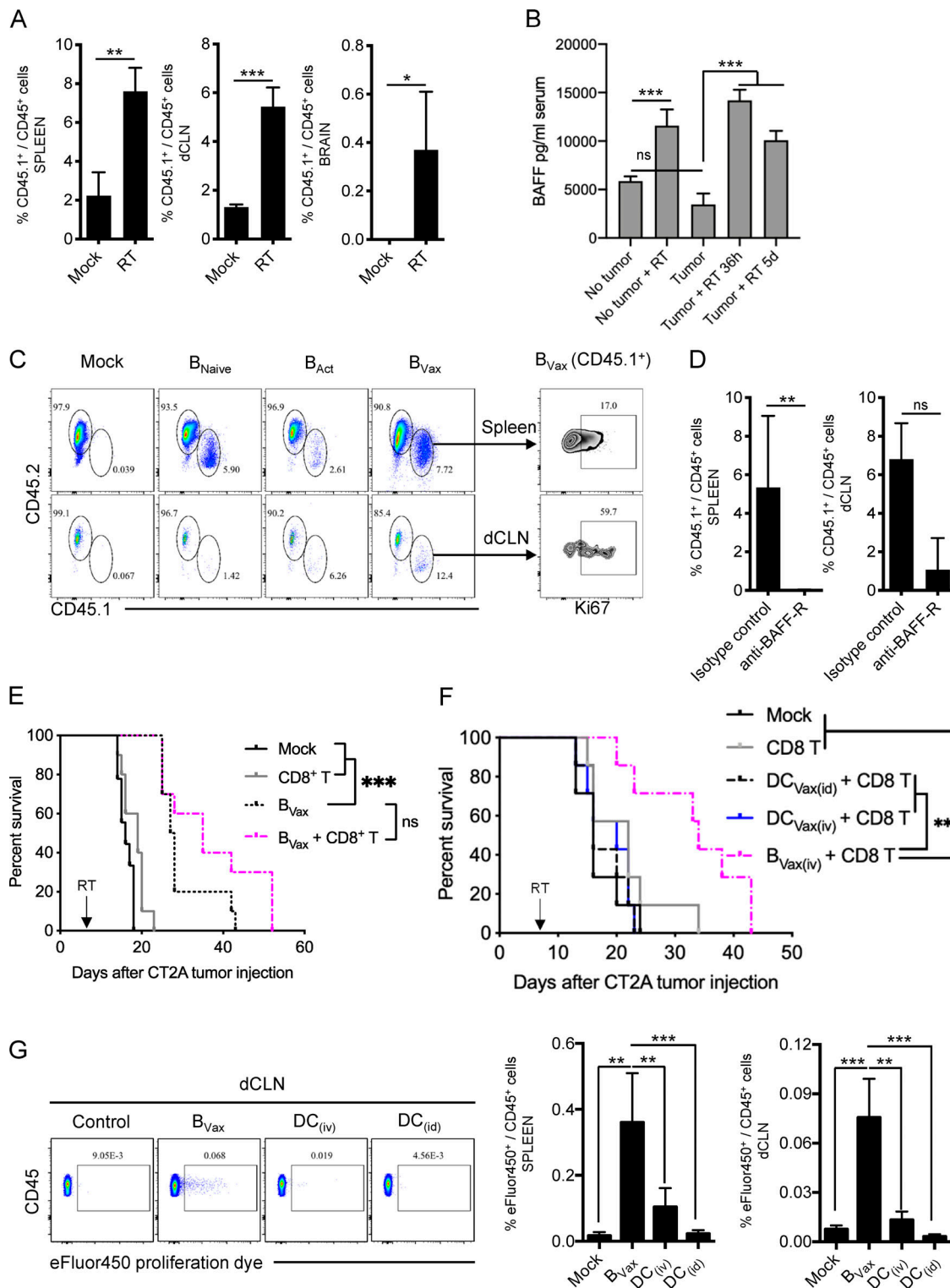
Figure 3. **Radiotherapy favors B cell adaption in vivo. (A)** CT2A-bearing mice were irradiated (RT), and CD45.1+ B_{Vax} were adoptively transferred i.v. CD45.1+ cells were analyzed by flow cytometry in the spleens, dCLNs, and tumor-bearing brains ($n = 4$ mice/group). **(B)** Irradiated CT2A-bearing mice were bled 36 h and 5 d after RTx ($n = 3$ mice/group). Serum BAFF levels were analyzed and compared with nonirradiated (Tumor) and non–tumor-bearing mice serum (No tumor). **(C)** The same experiment as in A was performed using CD45.1+ B_{Naive}, B_{Act} (4-1BBL− B cells activated with anti-CD40 and IFNγ), or B_{Vax}. CD45.1+ cells were analyzed by flow cytometry in the spleen and dCLN. B cell proliferative status was assessed by the expression of Ki67. A representative animal for each group ($n = 3$ or 4 mice/group) is depicted. The experiment was repeated twice independently. **(D)** Alternatively, a group of mice received B cells pretreated with BAFF-R–blocking Ab. The treatment was also administered to the mice i.v. for 3 consecutive d after B cell transfer. **(E)** Irradiated CT2A-bearing mice received i.v. vehicle (Mock, black line), CD8+ T cells (gray line), pulsed B_{Vax} (black dashed line), or combined pulsed B_{Vax} + CD8+ T cells (pink dotted line). The experiment was performed using $n = 10$ mice/group. A representative experiment of three independent experiments is shown. **(F)** Irradiated CT2A-bearing mice received

i.v. vehicle (Mock, black line), CD8$^+$ T cells (gray line), CD8$^+$ T cells i.v. + pulsed DC$_{Vax}$ administered either i.d. (DC$_{Vax(i.d.)}$; dashed black line) or i.v. (DC$_{Vax(i.v.)}$; blue line), or pulsed B$_{Vax}$ + CD8$^+$ T cells (pink dotted line). The experiment was performed using n = 10 mice/group. A representative experiment of two independent experiments is shown. **(G)** Irradiated CT2A-bearing mice received i.v. eFluor450-labeled B$_{Vax}$ or DCs. DCs were administered either i.v. (DC$_{(i.v.)}$) or i.d. (DC$_{(i.d.)}$). 7 d after cell transfer, eFluor450$^+$ cells were analyzed in the dCLN and spleen (n = 3 or 4 mice/group). A representative experiment of two independent experiments is shown. Differences between two groups were analyzed by Student's t test. Differences among multiple groups were evaluated using one-way ANOVA with post hoc Tukey's multiple comparisons test. Histograms are shown as mean ± SD. Survival curves were generated via the Kaplan-Meier method and compared by log-rank test, and multiple comparisons were adjusted using the Bonferroni method. Statistical significance is depicted as follows: *, P < 0.05; **, P < 0.01; ***, P < 0.001. ns, not statistically significant.

B$_{Vax}$ or DCs. 5 d after cellular adoptive transfer, tumor-bearing brains were collected and evaluated for the amount of proliferating CD8$^+$ T cells, measured by the expression of Ki67. As shown in Fig. 4 B, animals that received B$_{Vax}$ displayed a higher amount of Ki67$^+$CD8$^+$CD45.1$^+$ T cells.

Combination therapy provides long-term animal survival

Activation of B cells can lead to the up-regulation of the immunoregulatory molecule Programmed-death ligand 1 (PD-L1; Freeman et al., 2000). This is a shared feature of B$_{Vax}$, as ~50% of the cells at the time of animal injection express PD-L1 (Fig. S5 A). This phenomenon could lead to adverse effects of consecutive B$_{Vax}$ injections, as the acquisition of PD-L1 by B cells is associated with immunosuppressive functions in the context of cancers (Epeldegui et al., 2019; Guan et al., 2016; Lee-Chang et al., 2019). Thus, we hypothesized that adding anti–PD-L1 treatment could improve B$_{Vax}$ effector function and therapeutic outcome. First, we evaluated whether B$_{Vax}$ + anti–PD-L1 improved CD8$^+$ T cell persistence in CT2A-bearing mice after RTx. Naive CD8$^+$ T cells were fluorescently labeled with a lipophilic fluorescent dye (CellTracker). 7 d after adoptive transfer, mice were evaluated for CellTracker$^+$ CD8$^+$ T cell abundancy. Tumor-bearing brains, dCLNs, and spleens showed significantly increased counts of adoptively transferred CD8$^+$ T cells when B$_{Vax}$ was administered together with anti–PD-L1 (Fig. 4 C). Furthermore, immunophenotype analysis revealed that adoptively transferred CD8$^+$ T cells acquired a CD44$^+$CD62L^{Hi}IFNγ$^+$ memory phenotype in vivo (Fig. 4 D).

Next, CT2A-bearing mice received RTx and three i.v. injections of B$_{Vax}$ pulsed with CT2A lysates and CD8$^+$ T cells. After each cell therapy, mice were given an i.p. injection of anti–PD-L1 (500, 200, and 200 µg/mouse, respectively). This combination provided a significant clinical benefit, with 80% of mice being long-term survivors (LTSs; no RTx median survival days: 18; Mock (RTx): 25; anti–PD-L1: 28; CD8$^+$ T + anti–PD-L1: 39, B$_{Vax}$ + CD8$^+$ T + anti–PD-L1: undefined; anti–PD-L1 versus B$_{Vax}$ + CD8$^+$ T + anti–PD-L1: P < 0.0001; Fig. 5 A). 75 d after tumor injection, surviving mice were rechallenged with CT2A in the opposite hemisphere (Fig. 5 A, arrow). None of the mice developed any sign of tumor growth, and their clinical status was unchanged. After 245 d, surviving mice were sacrificed, and brains were evaluated for the presence of both tumor mass and CD8$^+$ T cells. Brain sections of LTSs treated with RTx, B$_{Vax}$, and CD8$^+$ T cells and PD-L1 blockade (LTS-B$_{Vax}$+CD8) were obtained from the right hemisphere (first site of injection, LTS-CD8+B$_{Vax}$ R) and left hemisphere (second site of injection, LTS-B$_{Vax}$+CD8 L). No sign of tumor mass, measured by H&E staining, was observed compared with age-matched control CT2A-bearing brains

sacrificed 14 d after tumor injection (Fig. 5 B). A majority of CD8$^+$ T cells in control tumor-bearing brains resided within the tumor vicinity, and minimal counts were found outside its boundaries (Fig. S5 B). In contrast, in LTS-B$_{Vax}$+CD8 animals that lacked tumor mass, CD8$^+$ T cells were found nearby the injection site but also at different locations, such as the choroid plexus, the pons, and the cerebellum. This CD8$^+$ T cell infiltration pattern was similar in both the right and left hemispheres (Fig. 5 C). Further immuno-profiling analysis revealed that the majority of the infiltrating immune cells in the brains of both LTS-CD8 and LTS-B$_{Vax}$+CD8 mice were CD8$^+$ T cells (Fig. 5 D). Furthermore, brain-infiltrating CD8$^+$ T cells from LTS-CD8+B$_{Vax}$ mice showed an activated IFNγ-expressing phenotype. Importantly, there was little-to-no expression of exhaustion and/or inhibitory molecules such as PD-1, KLGR1, or TIGIT in all LTS groups compared with CD8$^+$ T cells from tumor-bearing brains of the controls (Fig. 5 D). Only low amounts of myeloid cells or CD4$^+$ T cells were observed. Within the CD4$^+$ T cell compartment, the expression of Foxp3 was drastically reduced. Only LTS-B$_{Vax}$+CD8 brains showed increased accumulation of 4-1BBL$^+$IFNγ$^+$ B cells (Fig. S5 C), suggesting that B$_{Vax}$ treatment might also promote the accumulation of proinflammatory B cells. Altogether, the data demonstrate that the combination of RTx, B$_{Vax}$-based immunotherapy, and checkpoint blockade successfully eradicated the tumor. This clinical observation was associated with infiltration and persistence of functional CD8$^+$ T cells in the brain.

B$_{Vax}$ extend animal survival in combination with GBM SoC

Next, we evaluated the effect of B$_{Vax}$ treatment in combination with whole brain radiotherapy (B-RTx; total of 9 Gy, fractionated in three times 3 Gy) and TMZ (five i.p. injections of 50 mg/kg) in CT2A-bearing mice. Similar to whole-body RTx, serum BAFF levels were elevated in tumor-free and CT2A-bearing mice treated with TMZ, which was further increased when combined with B-RTx (Fig. 6 A). This suggests that SoC could promote B cell fitness in vivo. These results were associated with higher numbers of adoptively transferred CD45.1$^+$ B$_{Vax}$ in the spleen, dCLNs, and tumors of CT2A-bearing mice treated with SoC therapy (Fig. 6 B). B$_{Vax}$ therapeutic effectiveness was first evaluated in mice that were treated with either B-RTx (Fig. 6 C) or TMZ (Fig. 6 D). We observed that only B$_{Vax}$ in combination with CD8$^+$ T cells significantly extended animal survival after B-RTx treatment (Mock median survival: 20 d; B-RTx: 26; B-RTx + CD8$^+$ T: 26; B-RTx + B$_{Vax}$: 28, B-RTx + B$_{Vax}$ + CD8$^+$ T: 30; B-RTx versus B-RTx + B$_{Vax}$ + CD8$^+$ T: P = 0.01; Fig. 6 C). Similar results were obtained in tumor-bearing mice treated with TMZ (Mock median survival: 20 d; TMZ: 21; TMZ + CD8$^+$ T:
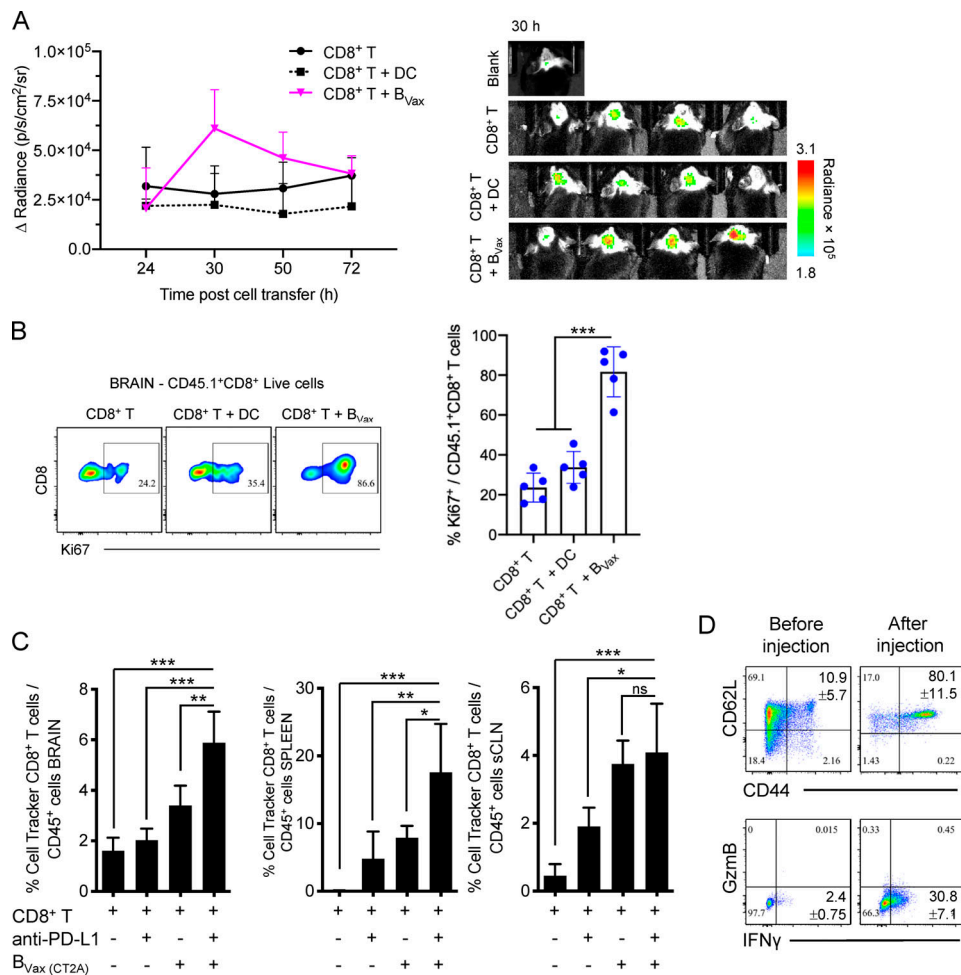
Figure 4. B$_{Vax}$ facilitates CD8$^+$ T cell tumor infiltration and proliferation. (A) CT2A-bearing mice were irradiated 7 d after tumor implantation. 48 h later, mice received i.v. DC or B$_{Vax}$ together with CellTracker Deep Red–labeled CD8$^+$ T cells. Far-red signal emitted by CD8$^+$ T cells was monitored at different time points (24, 30, 50, and 72 h). The experiment was performed using n = 4 mice/group. One mouse did not receive any lymphocytes and was used as a blank. In all experiments, mice were randomized and were grouped by treatment for the sole purpose of image capture. The fluorescence intensity was measured as photons per second per square centimeter per steradian (p/s/cm^2/sr). **(B)** Alternatively, mice received DC or B$_{Vax}$ (pulsed with CT2A lysates) concomitantly with CD8$^+$ T cells from CD45.1 congenic mice. 48 h later, mice were evaluated for the proliferative status of adoptively transferred CD45.1$^+$CD8$^+$ T cells by measuring the expression of Ki67. The experiment was performed using n = 5 mice/group. **(C)** CT2A-bearing mice were irradiated 7 d after tumor injection. 24 h after irradiation, mice received i.v. CellTracker Red CMPTX–labeled CD8$^+$ T cells ± B$_{Vax}$ pulsed with CT2A tumor lysates i.v. ± anti–PD-L1 i.p. 7 d later, CellTracker Red CMPTX–labeled CD8$^+$ T cell persistence (percentage of CellTracker$^+$ CD8$^+$T cells/total CD45$^+$ leukocytes) was analyzed by flow cytometry in the tumor-bearing brains, the dCLNs, and superficial CLNs (sCLNs). **(D)** Adoptively transferred CD8$^+$ T cells used in C were also phenotyped for CD44, CD62L, GzmB, and IFNγ in the dCLNs (after injection). The phenotype was compared with that before injection. The experiment was performed using n = 4 mice/group. For all experiments shown in this figure, differences among multiple groups were evaluated using one-way ANOVA with post hoc Tukey's test followed by post hoc Dunn's multiple tests. Histograms are shown as mean ± SD. Statistical significance is depicted as follows: *, $P < 0.05$; **, $P < 0.01$; ***, $P < 0.001$. ns, not statistically significant.

21; TMZ + B$_{Vax}$: 21.5; TMZ + B$_{Vax}$ + CD8$^+$ T: 27.5; TMZ versus TMZ + B$_{Vax}$ + CD8$^+$ T: $P < 0.0001$; Fig. 6 D).

Next, we tested the B$_{Vax}$ + CD8$^+$ T cellular therapy combination with both B-RTx and TMZ. A group of mice also received anti–PD-L1, as we observed previously that this checkpoint blockade strategy synergized with B$_{Vax}$ to eradicate the tumor (Fig. 5 A). For this experiment, mice received two consecutive injections of B$_{Vax}$ and CD8$^+$ T cells. After each cell therapy, mice were given an i.p. injection of anti–PD-L1. This combination provided a significant clinical benefit, with 50% of mice being LTSs (Mock median survival: 20 d; B$_{Vax}$ + CD8$^+$ T: 26; B-RTx + TMZ: 29; B-RTx + TMZ + B$_{Vax}$ + CD8$^+$ T: 38.5; RTx + TMZ +

anti–PD-L1: 32; RTx + TMZ + CD8$^+$ T + anti–PD-L1: 33; RTx + TMZ + B$_{Vax}$ + CD8$^+$ T + anti–PD-L1: 55; anti–PD-L1 versus B$_{Vax}$ + CD8$^+$ T + anti–PD-L1: $P < 0.0001$; anti–PD-L1 + CD8$^+$ T versus B$_{Vax}$ + CD8$^+$ T + anti–PD-L1: $P < 0.0001$; Fig. 6 E). Altogether, these data demonstrate that the combination of SoC strategy (B-RTx + TMZ), B$_{Vax}$-based cellular therapy, and PD-L1 checkpoint blockade significantly enhanced animal survival.

GBM patient-derived B$_{Vax}$ expand and activate autologous antiglioma CD8$^+$ T cells

Next, we tested the ability of GBM patient–derived B$_{Vax}$ to promote antitumor CD8$^+$ T cell response. 4-1BBL$^+$ B cells and
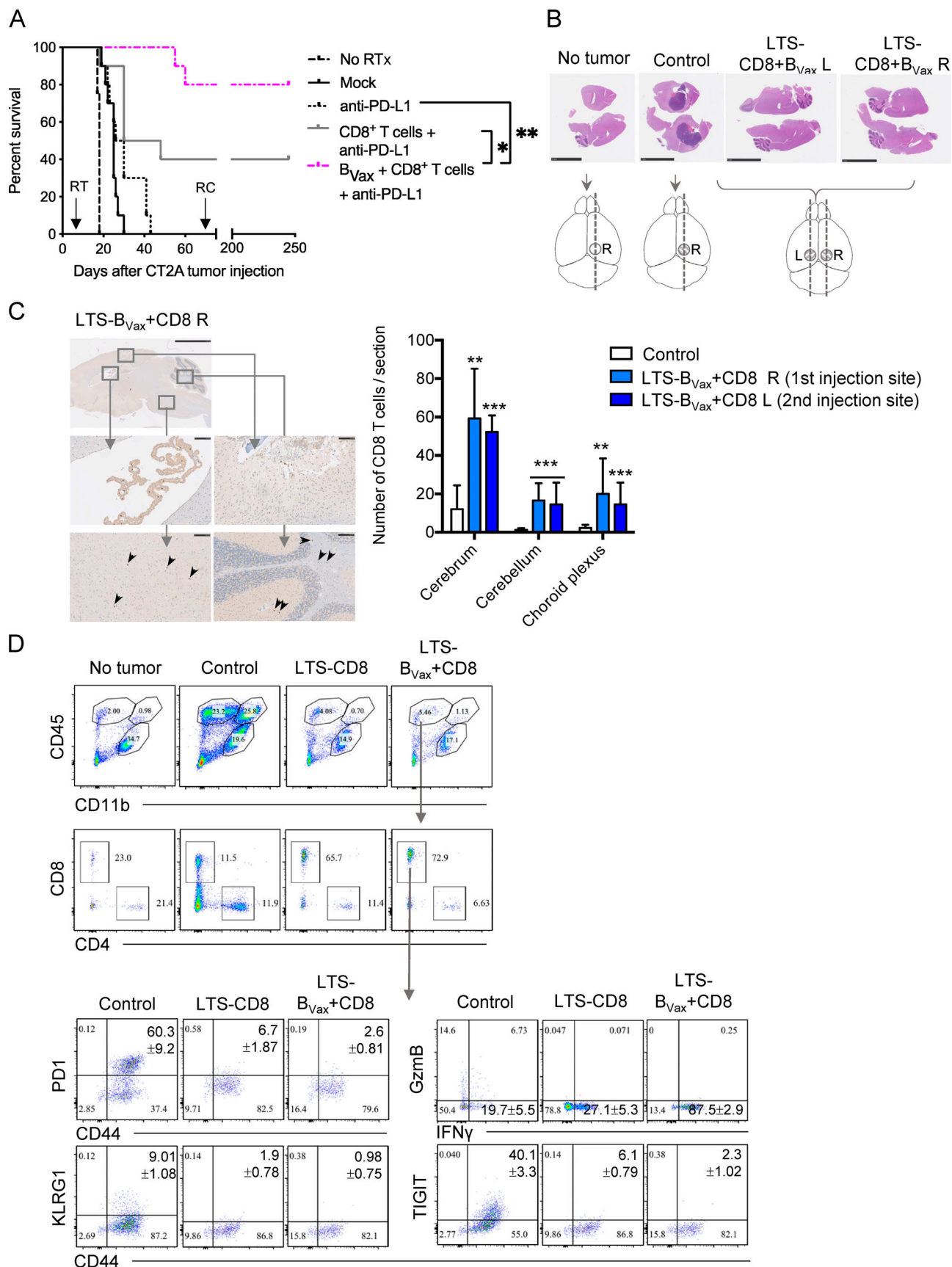
Figure 5. **B$_{Vax}$ potentiate the therapeutic effect of combined RTx + CD8$^+$ T + PD-L1 blockade. (A)** Irradiated CT2A-bearing mice received vehicle (Mock, black line), three injections of anti–PD-L1 (dotted black line), three injections of CD8$^+$ T cells and anti–PD-L1 (gray line), or three injections of pulsed B$_{Vax}$ +

CD8^{+} T cells and anti–PD-L1 (pink dotted line). A nonirradiated group was kept as control (No RTx, dashed black line). The experiment was performed using $n = 10$ mice/group. 75 d after tumor challenge (arrow marked RC), surviving mice were rechallenged (RC) with CT2A cells in the left hemisphere, opposite the initial tumor injection site. **(B)** LTSs were sacrificed and checked for the presence of tumor mass using H&E staining. Non–tumor-bearing but skull-drilled (no tumor) and age-matched CT2A-bearing mice (Control) were used as controls. Sections were performed as depicted in the cartoons. For LTSs treated with B_{Vax} and CD8^{+} T cells (LTS-B_{Vax}+CD8), brains were sectioned in both the right hemisphere (first site of injection, LTS-B_{Vax}+CD8 R) and the left hemisphere (second site of injection—rechallenge, LTS-B_{Vax}+CD8 L). H&E section images are representative of three LTS-B_{Vax}+CD8, two control, and one No tumor brains. Scale bars represent 5 mm. **(C)** The same brains used in B were used to stain for infiltrating CD8^{+} T cells. Representative images of one LTS-R section in which the choroid plexus, site of injection, the pons (arrowheads), and the cerebellum (arrowheads) are magnified. For the top image, bar represents 2.5 mm. For the magnified images, scale bars represent 100 µm. **(D)** Freshly dissected brains from No tumor ($n = 2$), Control ($n = 3$), LTSs that only received CD8^{+} T cells and PD-L1 blockade (LTS-CD8, $n = 4$), and LTS-B_{Vax}+CD8 ($n = 5$) mice were analyzed for lymphocyte phenotypes. Differences among multiple groups were evaluated using one-way ANOVA with post hoc Tukey's multiple comparisons test. Histograms are shown as mean ± SD. Survival curves were generated via the Kaplan-Meier method and compared by log-rank test, and multiple comparisons were adjusted using the Bonferroni method. Statistical significance is depicted as follows: *, $P < 0.05$; **, $P < 0.01$; ***, $P < 0.001$. ns, not statistically significant.

CD8^{+} T cells were isolated from GBM patient peripheral blood, followed by human B_{Vax} generation using the same protocol as murine B_{Vax}. We then used freshly resected tumor as a source of protein homogenate (tumor lysate) to pulse B_{Vax} (Fig. S5 D). The B_{Vax} (± tumor lysates) were tested for the ability to induce CD8^{+} T cell activation by coculturing pulsed B_{Vax} with autologous eFluor450-labeled CD8^{+} T cells. Cultures were supplemented with recombinant human IL-2, and no exogenous TCR stimulators such as anti–CD3/CD28 were added to the culture. We observed that CD8^{+} T cells cultured with B_{Vax} for 5 d expanded greatly and expressed high levels of GzmB. This observation was almost exclusive to B_{Vax} pulsed with autologous tumor lysates (expansion index mean percentage ± SD: B_{Vax} versus $B_{Vax(TUMOR LYSATE)}$ 3.1% ± 1.8% versus 6.05% ± 1.4%; $P < 0.05$; percentage of
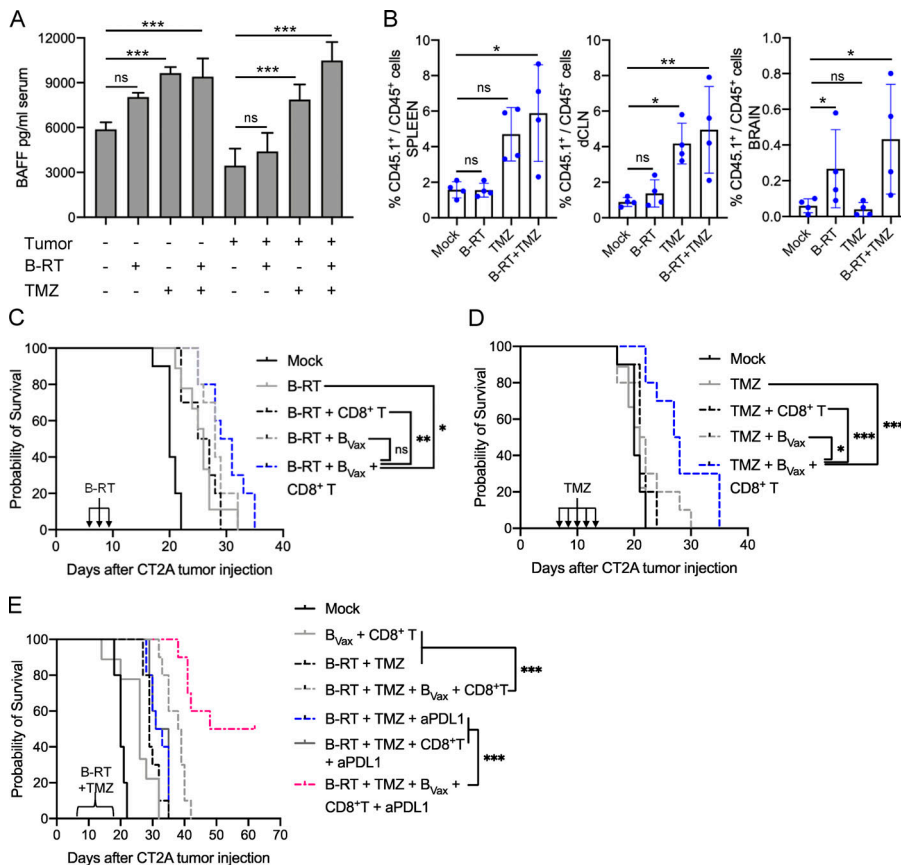

Figure 6. **B_{Vax}-enhanced animal survival in combination with GBM SoC and PD-L1 blockade. (A)** Mice received B-RTx for 3 consecutive d (D7–D10; 3 Gy each day) followed by 50 mg/kg of TMZ for 5 consecutive d (D11–D16). Serum BAFF levels were measured by ELISA 36 h after termination of the chosen therapy. Histograms are shown as mean ± SD. **(B)** B_{Vax} from congenic CD45.1[+] mice were adoptively transferred into CD45.2[+] CT2A-bearing mice ($n = 4$ mice/group). 7 d after cell adoptive transfer, CD45.1^{+} cells were analyzed by flow cytometry in the spleen, dCLNs, and tumor-bearing brains ($n = 4$ mice/group). **(C)** B_{Vax} ± CD8^{+} T cell therapeutic effect was tested in mice that received B-RTx. Non-irradiated (Mock, black line) and irradiated (B-RTx, gray line) mice were used as controls. Experimental groups received i.v. either CD8^{+} T cells (B-RTx + CD8^{+} T cells, dashed black line), B_{Vax} (B-RTx + B_{Vax}, dashed gray line), or both (B-RTx + B_{Vax} + CD8^{+} T cells, dashed blue line). The experiment was performed using $n = 10$ mice/group. **(D)** B_{Vax} ± CD8^{+} T cell therapeutic effect was tested in mice that were treated with TMZ. Untreated (Mock, black line) and TMZ-treated (TMZ, gray line) mice were used as controls. Experimental groups received i.v. either CD8^{+} T cells (TMZ + CD8^{+} T cells, dashed black line), B_{Vax} (TMZ + B_{Vax}, dashed gray line), or both (TMZ + B_{Vax} + CD8^{+} T cells, dashed blue line). The experiment was performed using $n = 10$ mice/group. **(E)** B_{Vax} + CD8^{+} T cell therapeutic effect was tested in mice treated with B-RTx and TMZ. Cellular therapy was administered 24 h after TMZ treatment termination (D19 after tumor challenge). Untreated mice (Mock, black line), mice that only received two i.v. injections of B_{Vax} + CD8^{+} T cells (B_{Vax} + CD8^{+} T, gray line), and irradiated mice that received TMZ (B-RTx + TMZ, dashed black line) were used as controls. Experimental groups treated with B-RTx and TMZ received two i.v. injections of B_{Vax} + CD8^{+} T cells (B-RTx + TMZ + B_{Vax} + CD8^{+} T, dashed gray line), two i.p. injections of PD-L1 blockade (aPD-L1; B-RTx + TMZ + aPDL1, dashed blue line), two i.v. injections of CD8^{+} T cells and two i.p. injections of PD-L1 blockade (B-RTx + TMZ + CD8^{+} T + aPDL1, gray line), or two i.v. injections of B_{Vax} + CD8^{+} T cells and two i.p. injections of PD-L1 blockade (B-RTx + TMZ + B_{Vax} + CD8^{+} T + aPDL1, dashed pink line). The experiment was performed using $n = 10$ or 11 mice/group. Differences among multiple groups were evaluated using one-way ANOVA with post hoc Tukey's test. Survival curves were generated via the Kaplan-Meier method and compared by log-rank test, and multiple comparisons were adjusted using the Bonferroni method. Statistical significance is depicted as follows: *, $P < 0.05$; **, $P < 0.01$; ***, $P < 0.001$. ns, not statistically significant.
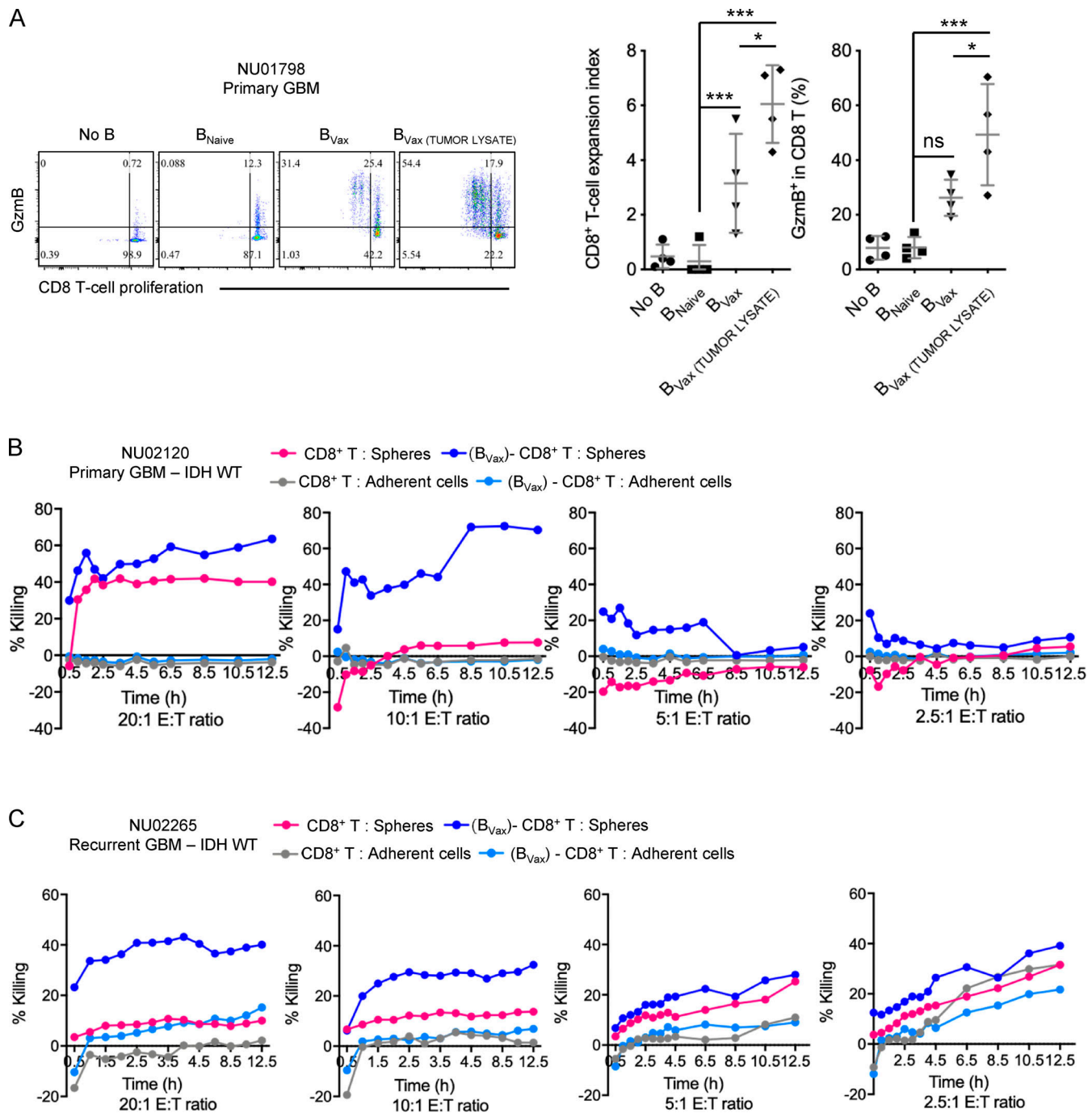
Lee-Chang et al.
B cell–based vaccine therapy of glioblastoma

Journal of Experimental Medicine
https://doi.org/10.1084/jem.20200913

11 of 23

Figure 7.   **GBM patient-derived B$_{Vax}$ promote anti-tumor CD8$^+$ T cells. (A)** Paired fresh peripheral blood and tumor were collected from newly diagnosed GBM patients (n = 4). B$_{Vax}$ were generated and pulsed with tumor lysates and co-cultured with autologous eFluor450-labeled CD8$^+$ T cells. CD8$^+$ T cell activation was assessed by cell proliferation (eFluor450 fluorescence dilution measured as expansion index) and intracellular expression of GzmB. **(B and C)** Paired samples from primary GBM isocitrate dehydrogenase (IDH) WT (case NU 02120, B) and recurrent GBM IDH WT (NU02265, C). B$_{Vax}$-activated autologous CD8$^+$ T cells (effector cells; E) were obtained as shown in A and tested for their ability to kill autologous glioma cells (target cells; T). Cell killing measurements were taken periodically for 12.5 h using the IncuCyte S3 Live Cell Analysis System. Differences among multiple groups were evaluated using one-way ANOVA with post hoc Tukey's test followed by post hoc Dunn's multiple tests. Histograms are shown as mean ± SD. Statistical significance is depicted as follows: *, P < 0.05; **, P < 0.01; ***, P < 0.001. ns, not statistically significant.

GzmB expression in mean ± SD: B$_{Vax}$ versus B$_{Vax(TUMOR LYSATE)}$ 26.2% ± 6.6% versus 49.3% ± 18.55%; P < 0.05; Fig. 7 A).

Lastly, we tested the activated and expanded CD8$^+$ T cell's ability to kill autologous tumor cells via an in vitro cytotoxicity

assay. Our results showed that CD8$^+$ T cells activated via the pulsed-B$_{Vax}$ system were able to potently kill glioma cells and spare nontumor adherent cells (Fig. S5 E), both in the context of newly diagnosed GBM (NU case 02120; Fig. 7 B) and recurrence

(NU case 02265; Fig. 7 C). These results confirm the potency of B_{Vax} to promote CD8$^+$ T cell–mediated antiglioma immunity.

B_{Vax} produce tumor-reactive Igs

After adoptive transfer, approximately half of B_{Vax} express CD138 (Fig. 8 A), also known as syndecan-1, a molecule expressed in terminally differentiated Ab-producing cells (McCarron et al., 2017). Thus, next we examined the humoral immune response of B_{Vax} and whether B_{Vax}-derived Abs participated in tumor clearance. To obtain B_{Vax}-derived Igs, B_{Vax} obtained from CT2A-bearing mice were i.v. injected into B KO CT2A-bearing mice. Control groups receiving B_{Naive} and B_{Act} were also added to the experiment. 2 wk later, mice were sacrificed, and serum was collected (Fig. 8 B). Serum samples were used to measure Ig subtypes using ELISA. We observed that B_{Naive} and B_{Act} predominantly produced IgM, while B_{Vax} mainly produced IgG1, IgG2a, and IgG2b (Fig. 8 C). In parallel, serum samples were tested for their reactivity to CT2A using immunofluorescence (IF) on CT2A-bearing brains from B KO mice. As these mice are deficient in mature B cells, they also lack endogenous Ig production. Serum B_{Vax}-derived IgG reactivity was higher in the tumor area (Fig. 8 D, T) than in healthy brain areas (Fig. 8 D, B) but did not colabel with CD11b$^+$ myeloid cells (Fig. 8 D), suggesting that B_{Vax} produce tumor-specific Abs.

To test whether these Abs can recognize tumor-associated Ags, we used the OVA-SIINFEKL system. B_{Vax} first were generated from GL261 tumor-bearing mice expressing OVA (GL261-OVA) and then were subsequently injected into GL261-OVA–bearing B KO mice. 2 wk after the cell adoptive transfer, serum IgGs were purified using Protein A/G columns. After protein concentration normalization, samples were tested for their SIINFEKL reactivity using ELISA. We included Abs from SIINFEKL-immunized mice as a positive control. We observed that SIINFEKL reactivity was significantly increased in B_{Vax}-derived IgG compared with B_{Naive}-derived IgG (Fig. 8 E).

Next, we tested whether B_{Vax}-derived IgG (B_{Vax} IgG) could control tumor growth. B_{Vax} IgGs were collected as previously described and intracranially injected (three consecutive times, 12.5 µg/injection). B_{Naive}-derived IgGs (B_{Naive} IgGs) were used as a control. B_{Vax} IgGs significantly extended animal survival (Mock median survival: 20 d; B_{Naive} IgG: 16; B_{Vax} IgG: 31.5; Mock versus B_{Vax} IgG: P = 0.017; Fig. 8 F). These results confirm that humoral effector functions play a role in B_{Vax} antitumor properties.

Discussion

In our previous work, we reported that in the CT2A glioma model, B cell depletion using rituximab had beneficial results only when B cells were depleted locally, sparing most of the peripheral B cells (Lee-Chang et al., 2019). In contrast, systemic B cell depletion does not reveal the same therapeutic effect. This highlights the possibility that B cells with distinct functions (anti- or pro-tumorigenesis) could be activated during tumor development. Accordingly, B cell infiltration and formation of ectopic follicles within the tumor microenvironment were recently associated with positive responsiveness to checkpoint blockade in melanoma and sarcomas (Cabrita et al., 2020;

Helmink et al., 2020; Petitprez et al., 2020). However, GBM does not allow these lymphoid structures to be formed within the tumor microenvironment, as GBM restricts B cell infiltration (Lee-Chang et al., 2019) and is characterized by lymphodepletion (Thorsson et al., 2018). However, some B cell subsets might still be able to promote an antitumor response. The 4-1BBL expression on B cells identifies Ag-experienced B_{Act} (Futagawa et al., 2002). It was previously shown that 4-1BBL$^+$ B cells express high levels of proinflammatory cytokines such as TNFα and costimulatory molecules such as CD86, which were shown to have a central role in CD8$^+$ T cell activation (Lee-Chang et al., 2016, 2014). In glioma-bearing mice, 4-1BBL$^+$ B cells were found increased in the peripheral lymphoid organs, and they differed from immunosuppressive B cells found in the tumor microenvironment (Lee-Chang et al., 2019). In GBM patients' peripheral blood, the association between the levels of 4-1BBL expression by B cells and the activation status of CD8$^+$ T cells (expression of CD69) suggested a possible proinflammatory immune signature within these patients. Further functional studies ex vivo confirmed that activation of CD8$^+$ T cells was related to 4-1BBL$^+$ B cells. Thus, we considered this rare but highly B_{Act} subset as a potential cellular platform to boost CD8$^+$ T cell–mediated tumor killing.

4-1BBL is the single known ligand for 4-1BB (Goodwin et al., 1993), a TNF receptor family costimulatory receptor that plays a fundamental role in activating Ag-experienced CD8$^+$ T cells to establish long-term immunological memory (Melero et al., 1997; Uno et al., 2006). Thus, 4-1BB agonism continues to be an attractive strategy to boost CD8$^+$ T cell immunity in the context of different cancers, including non-Hodgkin lymphoma and melanoma (Chester et al., 2018). 4-1BBL expression in B cells requires BCR and CD40 stimulation (Futagawa et al., 2002) and defines a specific subset of B_{Act} able to activate 4-1BB$^+$ CD8$^+$ T cells and promote antitumor immunity (Bodogai et al., 2015; Lee-Chang et al., 2016, 2014). Overexpression of 4-1BBL on the surface of APCs is transient and tightly controlled, as the aberrant presence of this marker might induce acute inflammation (Bukczynski et al., 2004; Vinay and Kwon, 1998). In our study, we used 4-1BBL$^+$ B cells from glioma-bearing mice (SLOs) or GBM patient–derived PBMCs as a source of B cell–based vaccine, or what we term B_{Vax}. In the aim of potentiating and stabilizing APC function, 4-1BBL$^+$ B cells were further activated for a short time (48 h) using CD40 and IFNγR activation and were pulsed with tumor protein lysates to generate the vaccine. Unlike naive B cells, B_{Vax} were able to cross-present as potently as DCs in vitro; thus, they could be considered a professional APC. This agrees with a previous study that showed that cross-presentation by B cells activates autoimmune CD8$^+$ T cells in the context of type 1 diabetes (Mariño et al., 2012). Most B cell–based vaccines use total B cells from peripheral blood. B cells are isolated using either CD19 or CD20 B-cell pan markers and activated ex vivo using CD40 agonism, Toll-like receptor ligands, homeostatic cytokines such as IL-4 or IL-21 (Wennhold et al., 2019). Some studies have used CD27$^+$ memory B cells (Jourdan et al., 2017). However, in this study, we showed that sorting Ag-experienced B cells (via 4-1BBL) and endowing them with potent APC function can be used as a unique tool in B cell–based therapies. However, a limitation of our study is the source of
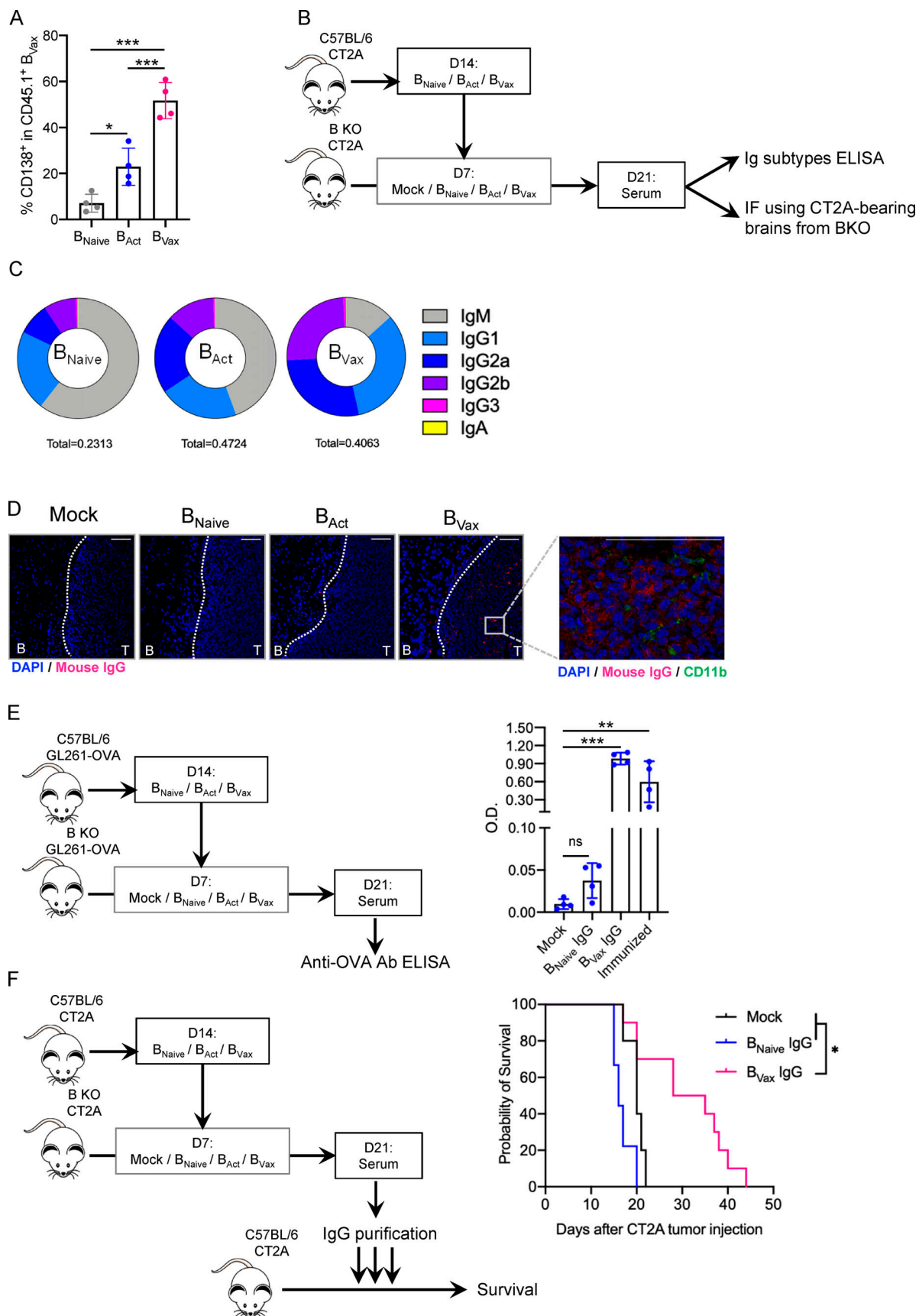
Figure 8. B$_{Vax}$ produce tumor-reactive Abs with therapeutic effect. (A) CD45.1$^+$ B$_{Vax}$ were adoptively transferred into B cell–deficient (B KO) CT2A-bearing mice. 72 h after, CD45.1$^+$ B$_{Vax}$ were evaluated for the expression of plasmablast marker CD138 by flow cytometry in the dCLN (n = 4/group).

(B) Schema of B$_{Vax}$-derived serum Ig obtainment. **(C)** Diagram representing the distribution of different Ig subtypes from serum Abs derived from B$_{Naive}$, B$_{Act}$, and B$_{Vax}$. Ig subtype measurement of serum samples was performed by ELISA, and mean total Ig concentration is shown in the bottom of the diagram (in milligrams per milliliter). The experiment was performed in seven mice/group. **(D)** B cell subset IgG reactivity was measured by IF. Serum samples were incubated on tumor-bearing brain sections from B cell–deficient mice (B KO). Binding IgG was detected using anti-mouse IgG Cy5 (red) secondary Ab. Nuclei were detected using DAPI (blue), and myeloid cells were evaluated by using anti-mouse CD11b AF488 Ab (green). Scale bars represent 100 μm. A representative experiment of serum obtained in 4 mice/group is shown, performed twice independently. **(E)** B$_{Naive}$, B$_{Act}$, and B$_{Vax}$ were generated from GL261-OVA tumor-bearing mice. B cells were allowed to produce Abs in GL261-OVA–bearing B KO mice. Serum samples were collected, and IgGs were purified and tested for their reactivity against OVA peptide SIINFEKL by ELISA. Semi-quantitative measurement is shown as optical density (OD). Sera from B cell–deficient mice and C57BL/6 SIINFEKL-immunized mice were used as negative and positive controls, respectively ($n = 4$/group). **(F)** Purified IgGs were tested for their therapeutic effect in the CT2A model. IgGs were delivered intracranially for 3 consecutive d (12.5 μg/mouse/injection). Untreated mice (black line) were used as controls. Experimental groups received either B$_{Naive}$-derived IgG (B$_{Naive}$ IgG, blue line) or B$_{Vax}$-derived IgG (B$_{Vax}$ IgG, pink line). The experiment was performed using $n = 10$ mice/group. Differences among multiple groups were evaluated using one-way ANOVA with post hoc Tukey's multiple comparisons test. Histograms are shown as mean ± SD. Survival curves were generated via the Kaplan-Meier method and compared by log-rank test, and multiple comparisons were adjusted using the Bonferroni method. Statistical significance is depicted as follows: *, $P < 0.05$; **, $P < 0.01$; ***, $P < 0.001$. ns, not statistically significant.

4-1BBL$^+$ B cells in the murine model and humans. We chose to use SLOs as a B$_{Vax}$ source in the preclinical setting because the volume of blood (and relative sparsity of 4-1BBL$^+$ B cells in the circulation) makes PBMC-generated B$_{Vax}$ from mice untenable.

In GBM patients, one consequence of radio- and chemotherapy is lymphopenia, which can be profound and persistent (Grossman et al., 2015, 2011; Nabors et al., 2011). A previous study showed that CD4$^+$ T and CD19$^+$ B cells are particularly affected by concomitant RT/TMZ administration (Ellsworth et al., 2014). These authors observed that T cell homeostatic factors such as IL-7 or IL-15 are unchanged, which suggests that in some patients, T cells are particularly vulnerable to SoC (Ellsworth et al., 2014). In a parallel study, it was observed that in RT/TMZ–induced lymphopenic patients, levels of B cell survival factor BAFF (also known as BLyS) were significantly elevated (Saraswathula et al., 2016), suggesting that the SoC might provide a more optimal environment for B cell adaption and persistence. This is clinically relevant, as an important limitation of current cell-based immunotherapy is its lack of persistence in vivo (DeRenzo and Gottschalk, 2019). Accordingly, RT-treated CT2A-bearing mice showed sustained increased levels of BAFF in the blood. BAFF is a universal homeostatic factor for all B cell subtypes. This observation was associated with the ability of all B cell subtypes tested (B$_{Naive}$, B$_{Act}$, and B$_{Vax}$) to persist in vivo. Treatment with BAFF-R–blocking Ab affected the survival of B$_{Vax}$ in vivo. Another interesting potential of B$_{Vax}$ is the determination of their BCR repertoire and, by extension, their Ab specificity. How these Abs might influence antiglioma immunity or tumor progression is a matter of ongoing study in our laboratory.

Tissue recruitment of B$_{Vax}$ is fundamental for their efficacy, as blockage of their migratory abilities toward SLOs abrogated their activating function of CD8$^+$ T cells. The dependency between CD8$^+$ T cells and B$_{Vax}$ was strongly supported by the in vivo tracking of CD8$^+$ T cells, in which their accumulation in the tumor-bearing brains was enhanced when B$_{Vax}$ was concomitantly administered. Optimal TCR stimulation by APC and subsequent T cell egress occurred 1–2 d after the interaction (Mempel et al., 2004). Accordingly, maximal accumulation of CD8$^+$ T cells in the brain was observed 30 h after cell B$_{Vax}$ + CD8$^+$ T cell injection. In support, B$_{Vax}$ therapeutic effect was significantly increased when administered concomitantly with CD8$^+$ T cells. One could hypothesize that the lack of B$_{Vax}$'s target cells

(CD8$^+$ T cells) driven by radio- and chemotherapy dampens the vaccine's therapeutic effect.

Like many immune cells, activated B cells express PD-L1, most likely as a mechanism to control inflammation. We used this as a rationale to combine B$_{Vax}$ and anti–PD-L1 immunotherapy. B$_{Vax}$ + anti–PD-L1 treatment promoted CD8$^+$ T cell persistence in vivo upon RTx in both tumor-bearing brains and draining CLNs. CD8$^+$ T cells showed a remarkable memory phenotype and expression of IFNγ, indicating an expansion of functional sentinel CD8$^+$ T cells. Consistent with this, repeated administration of B$_{Vax}$ and anti–PD-L1 allowed adoptively transferred CD8$^+$ T cells to eradicate the tumor and prevent its regrowth upon reinjection in the opposite hemisphere in 80% of the treated mice. Tumor eradication correlated with prominent infiltration of CD8$^+$ T cells in the injection sites (in both challenge and rechallenge sites). CD8$^+$ T cells were also found in the choroid plexus, a structure known to play a fundamental role in CNS immunosurveillance via the cerebrospinal fluid–brain barrier (Wilson et al., 2010). However, CD8$^+$ T cells were also present in more distant sites such as the cerebellum and pons, suggesting organwide surveillance to protect the CNS. Accordingly, CNS-infiltrating CD8$^+$ T cells show an activated phenotype characterized by the expression of IFNγ and CD44, together with the absence of inhibitory molecules such as PD-1 or TIGIT. These findings suggest that fully functional memory-like CD8$^+$ T cells persist in the target organ. Whether these cells arise from the adoptively transferred CD8$^+$ T cell pool or from newly differentiated cells upon lymphocyte replenishment due to RT-driven lymphopenia is a subject for future studies.

Accumulations of activated, oligoclonal B cells were found in tumors of metastatic melanoma patients who responded to immune checkpoint blockade in neoadjuvant treatment settings (Helmink et al., 2020). A B cell lineage gene signature also correlated with responsiveness to PD1 blockade in sarcoma patients (Petitprez et al., 2020). GBM patients show poor B cell infiltration within the tumor microenviroment. These B cells present a strong immunosuppressive profile (Lee-Chang et al., 2019). However, in our preclinical setting, LTSs treated with both B$_{Vax}$ and CD8$^+$ T cells showed an accumulation of proinflammatory 4-1BBL$^+$IFNγ$^+$ B cells in the brain. It remains to be seen whether this plays a role in enhancing CD8$^+$ T cell response in the context of PD-L1 blockade. It is also important to note that repeated CD8$^+$ T cell adoptive transfer (without B$_{Vax}$) and

anti–PD-L1 also eradicated the tumor in a small group of treated mice. These results suggest that a mechanism independent of B$_{Vax}$ is also taking place to promote CD8$^+$ T cell–mediated CNS immunosurveillance. We could hypothesize that anti–PD-L1 therapy could directly target tumor-associated myeloid cells, the most prominent nonneoplastic cell population in GBM (Zhang et al., 2019). Together with whole-body RTx, adoptively transferred CD8$^+$ T cells could thrive within the tumor microenvironment and kill GBM cells.

Similar to whole-body RTx, B-RTx + TMZ therapy promoted increased levels of serum BAFF, as seen in GBM patients who underwent SoC treatment (Sanchez-Perez et al., 2013; Saraswathula et al., 2016). Increased levels of serum BAFF correlated with enhanced B$_{Vax}$ persistence in vivo and with B$_{Vax}$ therapeutic effect. The combination of SoC, B$_{Vax}$ + CD8$^+$ T cells, and PD-L1 blockade provided tumor eradication in 50% of treated mice. However, unlike mice treated with whole-body RTx, little to no effect was seen in CD8$^+$ T cell (without B$_{Vax}$) + PD-L1 blockade in mice treated with whole-brain RTx. This suggests that GBM SoC provides a unique advantage for B cell–based therapies over adoptive transfer therapies alone.

Finally, we generated GBM patient–derived B$_{Vax}$ that, after pulsing with protein lysates originated from the freshly resected tumor from the same patient, activated and expanded autologous CD8$^+$ T cells. Those B$_{Vax}$-activated CD8$^+$ T cells killed autologous glioma cells and, at the same time, spared adherent cells. The fact that no exogenous activation (e.g., anti–CD3/CD28 activation) was required to induce CD8$^+$ T cell activation suggests that patient-derived B$_{Vax}$ present tumor-associated Ags to Ag-experienced CD8$^+$ T cells. In GBM patients, peripheral T cells share clonality with tumor-infiltrating lymphocytes (Sims et al., 2016), suggesting that tumor-specific T cells might be present in the circulation and that B$_{Vax}$ could be an ideal platform to expand these cells and boost their cytotoxic effect.

One major reason that B$_{Vax}$ outperformed DC therapeutic effect could be attributed to the unique ability of B cells to become Ab-producing cells in vivo and potentially produce antitumor humoral response. Our data show that B$_{Vax}$ produce mainly IgGs that react to tumor cells and tumor-associated Ags, which extend animal survival. Thus, B$_{Vax}$ might produce tumor-specific Abs able to cross the blood–brain barrier and attack tumor cells via Ab-dependent cell cytotoxicity. However, we also observed that B$_{Vax}$ can migrate and infiltrate the tumor. In addition, our results from LTSs show that a substantial amount of 4-1BBL$^+$IFNγ$^+$ B cells are present in brains 245 d after tumor implantation. Thus, one could hypothesize that tumor-infiltrating B$_{Vax}$ could seed an ectopic germinal center reaction and act as a source of Abs in situ. While further studies are needed to elucidate the exact reactivity of B$_{Vax}$ IgGs and their effector immune functions, it is undeniable that B$_{Vax}$ represents a unique immunotherapy platform that merges both cellular (CD8$^+$ T cell activation) and humoral (Ab production) functions.

Overall, our study proposes the use of 4-1BBL$^+$ B cells as a source of potent cellular and humoral immunotherapy. This is an autologous vaccine that only requires CD40 and IFNγR activation for a short time, which makes its clinical translation highly feasible.

Materials and methods

Human samples
All human samples (tumor, peripheral blood, and frozen tissue) were collected by the Nervous System Tumor Bank at Northwestern University under institutional review board protocol no. STU00202003. All patients signed written consent forms. Only samples from GBM patients with >50% tumor cellularity, as determined by H&E examination, were included in the study. The study was conducted following the U.S. Common Rule of ethical standards.

Mice
C57BL/6, CD45.1 C57BL/6, B KO (μMT), Rag1-deficient (Rag1 KO), and OT-I mice were all purchased from The Jackson Laboratory. 4-1BBL–deficient (4-1BBL KO) mice were obtained from Amgen. Animals were 6–8 wk old at initiation of the experiment. All animal experimentation protocols were approved by the Institutional Animal Care and Use Committee under protocol no. IS00002459 at Northwestern University. All animals were housed in a specific pathogen-free animal facility at Northwestern University.

Cell lines
GL261 cells were obtained from the National Cancer Institute. GL261 cells expressing OVA were obtained as previously reported in Pituch et al. (2018). CT2A cells were a gift from Prof. Tom Seyfried (Boston College, Boston, MA). GL261 cell line identity and purity were evaluated annually using short tandem repeats profiling performed by the Northwestern University sequencing core facility. Both murine syngeneic glioma cell lines were maintained in DMEM (Corning) with 10% FBS (HyClone), penicillin (100 U/ml), and streptomycin (100 mg/ml; Corning) and incubated at 37° in 5% CO_2. All cell lines were routinely tested for *Mycoplasma* contamination every 2 mo using the Universal Mycoplasma Detection Kit (ATCC 30-1012K).

Brain tumor injection
A total of 10^5 GL261 or CT2A cells were intracranially implanted as previously described (Wainwright et al., 2012a). Mice were anesthetized through i.p administration of a stock solution containing ketamine (100 mg/kg) and xylazine (10 mg/kg). The surgical site was shaved and prepared with a swab of povidone-iodine followed by 70% ethanol. The swabbing procedure was performed three times in total. An incision was made at the midline for access to the skull. A 1-mm–diameter burr hole was drilled 2 mm posterior to the coronal suture and 2 mm lateral to the sagittal suture. Mice were then placed in a stereotaxic frame, and tumor cells were injected in a total volume of 2.5 μl using a Hamilton syringe fitted with a 26-gauge blunt needle at a depth of 3 mm. The incision was then stapled closed.

Human immunophenotype analysis
Frozen PBMC samples (n = 90) from newly diagnosed GBM patients were collected and analyzed for levels of 4-1BBL-expressing B cells (4-1BBL$^+$CD20$^+$CD19$^+$) and CD69-expressing CD8$^+$ T cells by flow cytometry. The following antihuman Abs were used (all from BioLegend): 4-1BBL PerCP-Cy5.5 (5F4), CD19

Pacific Blue (HIB19), CD20 BV510 (2H7), CD8 Alexa Fluor 700 (RPA-T8), and CD69 PE-Cy7 (FN50). GzmB APC (GB11), IFNγ AF700 (4S.B3), and TNFα FITC (1D6) were used for intracellular staining. Dead cells and debris were excluded from the analysis using the eBioscience Fixable Viability Dye eFluor780 (Thermo Fisher). Cells were acquired by BD Symphony and analyzed by FlowJo software.

Murine immunophenotypic analysis

Tumor, blood, and lymph nodes were processed for immunotype purposes as previously described (Lee-Chang et al., 2019). Expression of 4-1BBL by B cells in blood, dCLNs, superficial CLNs, and tumor-bearing brains were analyzed by flow cytometry. Mouse Abs were all from BioLegend. CD45 BV510 (30F 11) and CD11b BV711 (ICRF44) were used to analyze the lymphocyte, myeloid, and microglia compartments. 4-1BBL PerCP-Cy5.5 (5F4) and CD19 BV650 (1D3/CD19) were used to evaluate the levels of 4-1BBL expression in B cells. Dead cells and debris were excluded from the analysis using the Fixable Viability Dye eFluor780 (Thermo Fisher). Cells were acquired by BD Symphony and analyzed by FlowJo software.

CD86 up-regulation using recombinant IFNγ

Human or murine B cells were isolated from PBMCs or spleens, respectively, and isolated using the Human or Mouse B Cell Isolation Kit (StemCell Technologies). Cells were resuspended at 2×10^6 cells/ml and incubated with 100 nM human (Peprotech) or murine (R&D) BAFF and 10 U/ml human or murine IFNγ. CD86 expression was assessed by flow cytometry using human anti-CD86 Pacific Blue (BU63; BioLegend) or anti-mouse CD86 AF700 (GL1) together with CD19 staining as described above.

Murine B$_{Vax}$ generation

B$_{Vax}$ were generated from 4-1BBL$^+$ B cells from spleens and dCLNs of tumor-bearing mice. Mice were challenged with 2×10^6 tumor cells and were sacrificed 12–14 d after tumor inoculation. B cells were negatively isolated from spleens and dCLNs using the EasySep Mouse B Cell Isolation Kit. 4-1BBL$^+$ cells were then magnetically positively isolated using anti-mouse 4-1BBL biotin (5F4; BioLegend) and antibiotin microbeads (Miltenyi Biotec). Cells were resuspended at 2×10^6 cells/ml of complete RPMI, supplemented with 100 nM of murine BAFF (R&D), and activated with anti-CD40 (FGK4.5; BioXCell). 24 h later, 10 U/ml of murine IFNγ was added to the culture. 48 h after the time of isolation, B$_{Vax}$ were harvested, counted, and ready for further utilization. In many experiments, B$_{Vax}$ were concomitantly injected with CD8$^+$ T cells that also originated from spleens and CLNs of tumor-bearing mice, isolated using the Mouse CD8$^+$ T Cell Isolation Kit (StemCell Technologies).

B$_{Vax}$ APC phenotype

Murine B$_{Vax}$ were tested for the expression of molecules associated with the APC function by flow cytometry. Cells were stained with the following anti-mouse Abs (all from BioLegend unless otherwise specified): IA^b PerCP-eFluor 710 (AF6-120.1), H-2K^b PE (AF6-88.5.5.3), CD86 AF700 (GL1), and 4-1BBL PerCP-Cy5.5 (5F4). After pulsing with 100 ng/ml SIINFEKL (Sigma-Aldrich),

the peptide presentation via H-2K^b was assessed using the anti-mouse SIINFEKL–H-2K^b PE-Cy7 (eBio25-D1.16; eBioscience).

B$_{Vax}$ APC function in vitro

To evaluate the ability of B$_{Vax}$ to uptake whole OVA, fluorescently labeled B$_{Vax}$ with CellTracker red CMPTX (Molecular Probes; Life Technologies) were incubated for 30 min with 15 µg/ml AF488-OVA (Molecular Probes; Life Technologies) in complete RPMI. Cells were washed three times and visualized with a Leica DMi8 microscope with a 40× objective. Data were processed and quantified using ImageJ. To evaluate the ability of B$_{Vax}$ to present SIINFEKL after whole OVA uptake, cells were incubated for 5 h with 1 µg/ml whole OVA (InvivoGen). SIINFEKL presentation by H-2K^b was assessed by flow cytometry as described above. To test the ability of whole OVA–pulsed B$_{Vax}$ to activate TCR transgenic OT-I CD8$^+$ T cells, splenic CD8$^+$ T cells were isolated using the Mouse CD8$^+$ T Cell Isolation Kit. We generated bone marrow–derived DCs as previously described (Miska et al., 2016) and used them as a positive control of cross-presentation. B$_{Naive}$ ($\pm$IFNγ), B$_{Vax}$, and DC pulsed with OVA protein were incubated at 1:1 ratio with CD8$^+$ T cells labeled with the Fixable Cell Proliferation Dye eFluor450 (eBioscience) and activated with anti-CD3/CD28 activating beads (Invitrogen) supplemented with recombinant IL-2 (30 U/ml; Peprotech). CD8$^+$ T cell activation was assessed by cellular proliferation (eFluor450 dilution) and intracellular expression of GzmB by flow cytometry. Alternatively, SIINFEKL peptides or CD8$^+$ T cells from WT C57BL/6 were used as the negative control. To test the involvement of Ag presentation via MHC class I, B$_{Vax}$ were pretreated with 10 µg/ml H-2K^b blocking Ab (clone AF6-88.5.5.3; BioXCell). The Ab was added every day throughout the experiment (72 h).

B$_{Vax}$ APC function in vivo

Rag1-deficient mice were orthotopically injected with 2×10^5 GL261-OVA. 7 d after tumor injections, mice were coinjected i.v. with both 2×10^6 B$_{Vax}$ cells (pulsed with whole OVA as described above) and 5×10^6 eFluor450-labeled CD8$^+$ T cells. 7 d after adoptive transfer, mice were sacrificed. Tumor-bearing brains and dCLNs were processed to obtain single-cell suspension as described in Lee-Chang et al. (2019). eFluor450$^+$ CD8$^+$ T cells were analyzed by flow cytometry. Alternatively, B KO µMT mice were orthotopically challenged with 10^5 GL261-OVA. 7 d after, mice received i.v. 2×10^6 whole OVA–pulsed B$_{Naive}$, B$_{Vax}$, or B$_{Vax}$ pretreated with 200 ng/ml *Bordetella pertussis* toxin (PTX; Gibco) for 1 h at 37°C. Of note, B$_{Vax(PTX)}$ were washed with PBS three times before injection. 7 d after B cell adoptive transfer, mice were sacrificed and SIINFEKL-specific CD8$^+$ T cells were analyzed by flow cytometry using the following anti-mouse Abs from BioLegend (unless otherwise specified): CD45 BV510 (30F 11), CD11b BV711 (ICRF44), CD8 BV605 (53–6.7), CD44 PerCP-Cy5.5 (IM7), and SIINFEKL–H-2K^b PE-Cy7 (eBio25-D1.16; eBioscience). In a parallel experiment, B KO µMT mice were challenged with 10^5 CT2A. 7 d after, mice received i.v. CT2A cell lysates–pulsed B$_{Naive}$, B$_{Vax}$, or B$_{Vax}$ + PTX. 7 d after B cell adoptive transfer, mice were sacrificed, and CD8$^+$ T cells were analyzed for the intracellular expression of GzmB and IFNγ using the following anti-mouse Abs, all from BioLegend: CD45 BV510

Lee-Chang et al.
B cell–based vaccine therapy of glioblastoma

Journal of Experimental Medicine   17 of 23
https://doi.org/10.1084/jem.20200913

(30F 11), CD11b BV711 (ICRF44), CD8 BV605 (53–6.7), GzmB AF647 (GB11), and IFNγ AF700 (XMG1.2). In all experiments, dead cells and debris were excluded from the analysis using the Fixable Viability Dye eFluor780. Cells were acquired by BD Symphony and analyzed by FlowJo software.

In vivo B_{Vax} tracking

B KO µMT mice were challenged with 10^5 CT2A. 9 d after, mice received i.v. 5×10^5 B_{Naive}, B_{Vax}, or B_{Vax} + PTX labeled beforehand with CellTracker red CMPTX. 3 d after, mice were sacrificed, and tumor-bearing brains, blood, and dCLNs were analyzed for the presence of CellTracker + CD19$^+$ B cells by flow cytometry as described above. Alternatively, tumor-bearing Rag1-deficient mice received i.v. and concomitantly both Cell-Tracker red CMPTX B_{Vax} cells and CellTracker Green CMFDA-labeled CD8$^+$ T cells. 3 d after the cell adoptive transfer, mice were sacrificed and spleens were collected. Tissue samples were embedded in O.C.T. (Thermo Fisher) and flash-frozen. Sections (6 µm) were obtained, and the presence of B_{Vax} (red cells) and CD8$^+$ T cells (green) were analyzed by fluorescent microscopy (Leica DMi8). Data were processed and quantified using ImageJ.

Serum BAFF measurement by ELISA

Mice were bled retro-orbitally, and samples were allowed to clot by leaving them at room temperature for 30 min. Clots were removed by centrifuging at 1,000–2,000 g for 10 min at 4°C. Sera were stocked at –80°C until use. BAFF levels were measured using the Mouse BAFF/BlysTNFSF13B Quantikine ELISA Kit (R&D) as directed by the manufacturer.

In vivo B_{Vax} adaptation upon radiation

WT C57BL/6 mice were intracranially challenged with 10^5 CT2A cells. After 7 d, mice received total body irradiation (9 Gy) using a Gammacell 40 Exactor (Best Theratronics). 2 d after, mice received i.v. 5×10^6 B_{Vax} originated from CT2A-bearing CD45.1 mice. 7 d after cell adoptive transfer, CD45.1$^+$ B_{Vax} were evaluated in the spleen, dCLNs, and tumor-bearing brains by flow cytometry using the anti-mouse CD45.1 eFluor450 (A20) and total CD45 PE (30-F11) from BioLegend. Alternatively, CD45.1$^+$ B_{Naive}–activated 4-1BBL$^-$ B cells with anti-CD40 and IFNγ (B_{Act}) and B_{Vax} were measured by flow cytometry using CD45.1 eFluor450 (A20) and CD45.2 PE-Cy7 (104). A group of mice received B_{Vax} treated with 10 µg/ml BAFF-R–blocking Ab (7H22-E16; BioLegend). Mice subsequently received 100 µg of BAFF-R–blocking Ab i.p. every day for 7 d. In vivo B cell proliferation was assessed by the expression of Ki67 (PE; BioLegend). Lymphopenia in irradiated mice was assessed by the numbers of CD45$^+$ leukocytes in the blood and spleen 5 d after irradiation. In a parallel experiment, 2×10^6 DCs and B_{Vax} labeled with Fixable Cell Proliferation Dye eFluor450 were injected i.v. A group of mice received an i.d. injection of DCs. 7 d after cell adoptive transfer, mice were sacrificed, and cell proliferation was assessed by flow cytometry as the dilution of eFluor450 dye within the CD45$^+$ cell population in the dCLNs and spleens.

B_{Vax} therapeutic effect

C57BL/6 mice were intracranially injected with 10^5 CT2A cells. After 7 d, mice received total body irradiation (9 Gy) using a Gammacell 40 Exactor. 2 d after, mice received i.v. 1.5×10^6 B_{Vax} $\pm$ 4–5×10^6 CD8$^+$ T cells isolated and processed as described above.

Alternatively, B KO mice were intracranially injected with 10^5 CT2A cells. After 9 d, mice received i.v. 1.5×10^6 B_{Naive}, B_{Act}, or B_{Vax} + 4–5×10^6 CD8$^+$ T cells isolated and processed as described above. In a parallel experiment, B_{Vax} were pretreated with 10 µg/ml of 4-1BBL blocking Ab (clone TKS-1; BioXCell) before injection, and mice received two i.p. injections of 500 µg/kg.

In vivo CD8$^+$ T cell tracking imaging

The Spectral Lago live small-animal imaging system was used to determine the in vivo trafficking of CD8$^+$ T cells to the brain of glioma-bearing mice. 7 d after tumor implantation, mice received whole-body irradiation as described above (9 Gy). 48 h after, each mouse received i.v. 5×10^6 CellTracker Deep Red–labeled CD8$^+$ T cells with 1.5×10^6 B_{Vax} (i.v.) or 1.5×10^6 DC (i.d.). At scheduled time points (24, 30, 50, and 72 h after cell adoptive transfer), the mice were anesthetized and scanned with excitation at 640 nm and emission at 690 nm. The fluorescence intensities in regions of interest were calculated using Aura Imaging Software.

Radiation, B_{Vax}, CD8$^+$ T cells, and anti–PD-L1 combination therapy

To evaluate the persistence and memory phenotype of adoptively transferred CD8$^+$ T cells in mice receiving the combination of RTx, B_{Vax}, and anti–PD-L1, WT C57BL/6 mice were challenged with 2×10^5 CT2A cells intracranially and were used as donors of B_{Vax} and CD8$^+$ T cells. Host mice received 10^5 CT2A cells intracranially. 7 d after, mice received total body irradiation (9 Gy; Gammacell 40 Exactor). 2 d later, mice received 2×10^6 B_{Vax} pulsed with CT2A protein homogenates (generated as described above), and 3×10^6 CellTracker PE CMTX-labeled CD8$^+$ T cells were injected i.v. 24 h later, mice received i.p. 500 µg/mouse of anti–PD-L1 (10F.9G2; BioXCell). 10 d after, mice were sacrificed and CellTracker$^+$CD8$^+$ T cells were analyzed by flow cytometry. The following anti-mouse Abs (BioLegend) were used to analyze the adoptively transferred CD8$^+$ T cells: CD45 BV510 (30F 11), CD11b BV711 (ICRF44), CD8$^+$BV605 (53–6.7), CD44 PerCP-Cy5.5 (IM7), CD62L BV421 (MEL-14), (53–6.7), and CD44 PerCP-Cy5.5 (IM7).

To test the effect of RTx, B_{Vax}, CD8$^+$ T cells, and anti–PD-L1 in animal survival, mice received total body irradiation (9 Gy; Gammacell 40 Exactor) 7 d after tumor implantation. 48 h after, mice received 1.5×10^6 B_{Vax} pulsed with CT2A protein homogenates ($B_{Vax(CT2A)}$) and 2×10^6 CD8$^+$ T cells i.v. 24 h after, mice received i.p. 500 µg/mouse of anti–PD-L1. After 2 d, mice received a second cycle of $B_{Vax(CT2A)}$+CD8$^+$ T cells followed by 200 µg/mouse of anti–PD-L1. After 2 d, mice received the third cycle of $B_{Vax(CT2A)}$+CD8$^+$ T cells followed by 200 µg/mouse of anti–PD-L1. 75 d after tumor injection, surviving mice were rechallenged in the opposite hemisphere (left) to the initial injection site with 10^5 CT2A cells intracranially.

Histopathological and immunophenotype analysis of LTSs' brains

LTSs were monitored daily. Mice were sacrificed 245 d after initial tumor injection. Three brains were formalin-fixed for

24 h at room temperature. The injection needle track was identified, and sagittal sectioning was performed for every mouse brain. For LTSs, brains were cut in the right and left hemispheres. Tissue samples were paraffin-embedded for immunohistochemistry evaluation. Age-matched (10-mo-old) control mice were sacrificed 14 d after CT2A tumor injection (10^5 cells/mouse intracranially). Tumor burden was analyzed by H&E staining. To evaluate CD8$^+$ T cell infiltration, sections were stained with anti-mouse CD8 (1/100 dilution; clone 4SM16; eBioscience) and donkey anti-rat IgG (Jackson Immuno-Research). The histopathological processing of the samples was performed at the Mouse Histology and Phenotyping Laboratory at Northwestern University. Five brains were used for the immune cell's phenotype. For immunophenotype analysis of brain-infiltrating immune cells, brain and peripheral tissue samples were processed as previously described in Lee-Chang et al. (2019). Cells were stained for the following anti-mouse Abs (from BioLegend): CD45 BV510 (30F 11), CD11b BV711 (ICRF44), CD4 PE-Cy7 or AF700 (GK1.5), CD8b FITC (YTS156.7.7) or CD8 BV605 (53–6.7), CD44 PerCP-Cy5.5 (IM7), CD44 PerCP-Cy5.5 (IM7), KLRG1 APC (2F1/KLRG1), TIGIT PE-Cy7 (1G9), PD-1 FITC (29F.1A12), Foxp3 BV421 (FJK-16S), CD19 PE or BV605 (1D5), 4-1BBL PerCP-Cy5.5 (TKS-1), and LAP/TGFβ PE (TW7-16B4).

Whole-brain radiation, TMZ and B$_{Vax}$, CD8$^+$ T cells, and anti–PD-L1 combination therapy

Alternatively, C57BL/6 mice were intracranially injected with 10^5 CT2A cells. After 7 d, mice brains were irradiated with a total of 9 Gy (fractionated three times 3 Gy; Gammacell 40 Exactor). At day 11 after tumor injection, mice received i.p. 50 mg/kg of TMZ for 5 consecutive d. 24 h after the last TMZ dose, mice received 1.5×10^6 B$_{Vax}$ ± 4–5×10^6 CD8$^+$ T cells isolated and processed as described above.

Patient-derived B$_{Vax}$ generation and autologous CD8$^+$ T cell activation assay

GBM patients' peripheral blood samples were collected in EDTA-treated tubes, and PBMCs were isolated by Ficoll gradient (GE Healthcare). PBMC B cells were obtained using the EasySep Human B Cell Isolation Kit II (StemCell Technologies). 4-1BBL–expressing B cells were then magnetically isolated using the human anti–4-1BBL biotin (BioLegend) and then antibiotin microbeads. 4-1BBL–expressing B cells were resuspended at 2×10^6 cells/ml in complete RPMI and stimulated with 5 μg/ml human anti-CD40 (clone, FGK4.5). After 24 h, 10 U/ml of recombinant human IFNγ (Peprotech) was added. Cells were incubated for an additional 24–48 h. B cells were supplemented with 100 nM of recombinant human BAFF throughout the entire in vitro activation process. T cells were isolated using the EasySep Human T-Cell Isolation Kit (StemCell Technologies) and labeled with 10 μM of the eBioscience Cell Proliferation Dye eFluor450 (Thermo Fisher). Cells were activated with T cell activator anti–CD3/CD28 beads (Dynabeads, Invitrogen; Thermo Fisher) at 1:3 beads:T cell ratio supplemented with IL-2 (50 U/ml) and cocultured at a 1:1 ratio with tumor-infiltrating or PBMC CD19$^+$ B cells for 72 h. CD8$^+$ T cell proliferation (eFluor450 dilution) and activation status (intracellular

GzmB and IFNγ expression) were analyzed using flow cytometry.

Human B$_{Vax}$-mediated autologous CD8$^+$ T cell activation and tumor cell killing assays

Freshly resected tumor samples were diced using a razor blade and incubated for 30 min at 37°C in a tissue culture dish (100-mm diameter) with digestion buffer, consisting of 4 ml of HBSS (Gibco) supplemented with 8 mg of collagenase D (Sigma-Aldrich), 80 μg DNase I (Sigma-Aldrich), and 40 μg $N_α$-Tosyl-L-lysine chloromethyl ketone hydrochloride (TLCK;Sigma-Aldrich) per ~2 g of the tumor sample. The sample was mixed by pipetting up and down several times every 10 min. Then, the cell suspension was mechanically dissociated using a tissue homogenizer (Potter-El-vehjem polytetrafluoroethylene pestle) in HBSS. Cells were cultured ex vivo as tumor spheroids in Neurobasal Medium with 1% B27 supplement, 0.25% N2 supplement, 1% penicillin streptomycin, 1 μg/ml heparin, 20 ng/ml human basic fibroblast growth factor, and 20 ng/ml human epidermal growth factor. Peripheral blood was processed by density gradient separation (Ficoll) to obtain PBMCs.

For tumor lysate preparation, tumor single-cell suspension was resuspended at 10^6 cells/ml of PBS and underwent five freeze-thaw cycles and 1 min of sonication.

B$_{Vax}$ generation

B cells were isolated using the Human B Cell Isolation Kit. 4-1BBL$^+$ B cells were magnetically isolated using anti-human 4-1BBL biotin (clone 5F4; BioLegend) and antibiotin microbeads. Cells were cultured at 2×10^6 cells/ml of complete RPMI (cRPMI) supplemented with 5 μg/ml anti-CD40 (clone 5C3; BioLegend) and 100 nM of recombinant human BAFF (R&D). 24 h after, 1,000 U/ml of recombinant IFNγ was added to the culture for an additional 18–20 h. B$_{Vax}$ were pulsed with tumor lysates for 5 h at 37°C. Cells were washed twice with cRPMI.

CD8$^+$ T cell activation assay

After PBMC isolation, CD8$^+$ T cells were isolated using the Human CD8$^+$ T Cell Isolation Kit (StemCell Technologies) and cultured with 30 U/ml of recombinant IL-2 for 24 h, until B$_{Vax}$ were generated and pulsed with tumor lysates. CD8$^+$ T cells were labeled with the Fixable Cell Proliferation Dye eFluor450 and mixed with B$_{Vax}$ at a 1:1 ratio supplemented with 30 U/ml of recombinant IL-2. CD8$^+$ T cell activation was assessed by flow cytometry as cell proliferation (dilution of eFluor450 dye) and expression of intracellular GzmB.

Tumor cell cytotoxicity assay

To assess activated CD8$^+$ T cell cytotoxic capabilities after co-culture with B$_{Vax}$, CD8$^+$ T cells were magnetically isolated using anti-CD8 biotin (clone SK1; BioLegend) and antibiotin microbeads. Of note, magnetic isolation was performed in both control (no B$_{Vax}$) and B$_{Vax}$-treated groups. Isolated CD8$^+$ T cells were added at various effector:target ratios with labeled ex vivo tumor cells, and cytotoxicity was assayed using the IncuCyte S3 Live Cell Analysis System (Sartorius; Essen BioScience). Tumor cells were prelabeled with CFSE according to the manufacturer's

Lee-Chang et al.
B cell–based vaccine therapy of glioblastoma

Journal of Experimental Medicine   19 of 23
https://doi.org/10.1084/jem.20200913

protocol and cultured in 96-well plates with 250 nM IncuCyte Cytotox Red Reagent with or without the addition of effector cells at 20:1, 10:1, 5:1, and 2.5:1 effector:target cell ratios. Assay controls to account for spontaneous target cell death (target cells alone) and maximum cell death (target cells + 0.1% Triton X) were included to allow for quantification of cell killing. Live cell images (four per well, with 10× objective) were taken at 30-min intervals from hour 0 to 2.5 and at 1-h intervals thereafter until completion of the assay at 12.5 h after plating. For image analysis, 5% green fluorescence was removed from the red channel, and quantification was performed at each experimental condition as a ratio of the [total red count] to [total green cell count]. The total red count is indicative of cell death, and the total green cell count is indicative of viable cells and cell proliferation over the course of the assay. To calculate percent killing of each condition (relative to the scale set by spontaneous and maximum cell death controls), the following calculation was performed at each condition: % Killing = (% Experimental – % Spontaneous) / (% Maximum Release – % Spontaneous) × 100. IncuCyte Live Cell Analysis was performed in the Analytical bioNanoTechnology Core Facility of the Simpson Querry Institute at Northwestern University. This core facility is currently supported by the Soft and Hybrid Nanotechnology Experimental Resource (NSFECCS-1542205).

B_{Vax}-derived Ig ELISA
B cell subset–derived Ig subtypes were measured using the Ig Isotyping Mouse Instant ELISA Kit (Invitrogen; Thermo Fisher).

Brain section IF using B_{Vax}-derived Ig
CT2A-bearing B KO mice were sacrificed 14 d after tumor injection. Mice were perfused with chilled PBS, and brains were collected and frozen in O.C.T. (Sakura). Brain tissue sections were fixed with prechilled methanol for 10 min at –20°C. Sections were washed and rehydrated for 20 min at room temperature with PBS and blocked with 1% BSA in PBS + 5% normal donkey serum for 1 h at room temperature. Mice serum was diluted at 1:10 in 0.1% BSA in PBS and applied on the section without washing the blocking buffer. Sections were incubated for an additional 2 h at room temperature, washed three times with PBS, and stained with secondary anti-mouse IgG Cy5 (Jackson ImmunoResearch) diluted 1:500 in 0.1% BSA in PBS for 45 min at room temperature. Slides were washed three times with PBS and mounted with Fluoroshield with DAPI (Sigma-Aldrich).

B_{Vax}-derived Ig purification
Mice serum IgGs were isolated using the NAb Protein A/G Spin Column (Thermo Fisher). Eluted proteins were concentrated using the Amicon Ultra 15-ml 30K (Millipore Sigma). Final IgG concentration was measured by the Bradford method.

SIINFEKL-reactive B_{Vax} Ig ELISA
ELISA 96-well microplates (Corning; Sigma-Aldrich) were coated overnight at 4°C with 10 µg/ml of SIINFEKL (Sigma-Aldrich) diluted in PBS. Plates were washed three times with PBS containing 0.05% Tween-20 to remove unbound SIINFEKL.

A volume of 100 µl PBS-BSA 1% was used for blocking for 1 h at room temperature. 50 µl per well of diluted IgG sample was added to corresponding wells in duplicate. The plates were incubated at room temperature for 1 h and washed three times. To measure OVA-specific Ab, anti-mouse IgG coupled to peroxidase was added to wells at the dilution of 1:1,000 (Thermo Fisher). Secondary Abs were incubated for 1 h at room temperature. Plates were washed three times, and 50 µl of streptavidin coupled with horse-peroxidase was added to the plates and incubated at room temperature for 20 min. After three washes, the signal was revealed by adding 50 µl tetramethylbenzidine, and the plates were incubated at room temperature for 15 min in the dark. The reaction was stopped by adding 25 µl H_2SO_4 2N. Optical density at 492 nm was measured using the Genemate Uniread 800 plate reader.

B_{Vax}-derived Ig therapeutic effect
B KO mice received 10^5 CT2A cells intracranially using a cannula system. Briefly, mice were anesthetized, and a skin incision ~10 mm in length was made over the middle frontal to the parietal bone to expose the surface of the skull. A 26-gauge sterile guide cannula for mice (Plastics One) was installed into the mouse brain at 2-mm depth through the burr hole generated during tumor implantation, as described above. Tissue glue was applied around the burr hole to secure the protrusion of the cannula for long-term stable positioning. The scalp was closed with surgical glue around the implantation site. A protection dummy cannula was used to secure the protrusion end during the postop recovery and following observation period. For anti-CD20 injection, a 33-gauge sterile syringe was inserted into the guide cannula. The syringe can be covered with a sleeve designed to extend 1 mm beyond the tip of the guide cannula. Purified serum IgG (12.5 µg/mouse/injection) was injected into the brain (final volume of 2.5 µl/injection). After injection, the cannula was covered using a 33-gauge dummy cannula for mice.

Statistical analysis
Data are shown as mean ± SD for a continuous variable and number (percentages or optical density measures) for a categorical variable. Differences between two groups were analyzed by Student's t test. Differences among multiple groups were evaluated using one-way ANOVA with post hoc Tukey's mutiple comparisons test. Survival curves were generated via the Kaplan-Meier method and compared by log-rank test, and multiple comparisons were adjusted using the Bonferroni method. Categorical variables were analyzed using Fisher's exact tests or χ^2 tests as appropriate. All the tests are two-sided, and P values or Benjamini-Hochberg adjusted false discovery rates <0.05 were considered significant. Statistical analyses were performed using SAS9.4 and GraphPad Prism 7.03.

Online supplemental material
Fig. S1 indicates the expression levels of 4-1BBL by B cells in tumor-bearing brains and SLOs over time in the CT2A model, indicating the fundamental role of 4-1BBL in B cell–mediated CD8 T cell activation. Fig. S2 depicts the protocol for B_{Vax} generation. Fig. S3 shows that 4-1BBL is a key marker for B_{Vax} therapeutic

Lee-Chang et al.
B cell–based vaccine therapy of glioblastoma

Journal of Experimental Medicine 20 of 23
https://doi.org/10.1084/jem.20200913

effect. Fig. S4 shows B_Vax therapeutic effect in combination with whole-body irradiation. Fig. S5 indicates that B_Vax-treated LTSs' brains present with a significantly low amount of CD4$^+$ T cells and high counts of activated 4-1BBL$^+$IFNγ$^+$ B cells, with depiction of the protocol to produce GBM-derived B_Vax and its ability to promote autologous anti-tumor CD8$^+$ T cells.

References

Ahmadi, T., A. Flies, Y. Efebera, and D.H. Sherr. 2008. CD40 Ligand-activated, antigen-specific B cells are comparable to mature dendritic cells in presenting protein antigens and major histocompatibility complex class I- and class II-binding peptides. *Immunology*. 124:129–140. https://doi.org/10.1111/j.1365-2567.2007.02749.x

Bodogai, M., K. Moritoh, C. Lee-Chang, C.M. Hollander, C.A. Sherman-Baust, R.P. Wersto, Y. Araki, I. Miyoshi, L. Yang, G. Trinchieri, et al. 2015. Immunosuppressive and Prometastatic Functions of Myeloid-Derived Suppressive Cells Rely upon Education from Tumor-Associated B Cells. *Cancer Res*. 75:3456–3465. https://doi.org/10.1158/0008-5472.CAN-14-3077

Braun, D., I. Caramalho, and J. Demengeot. 2002. IFN-alpha/beta enhances BCR-dependent B cell responses. *Int. Immunol*. 14:411–419. https://doi.org/10.1093/intimm/14.4.411

Bruno, T.C., P.J. Ebner, B.L. Moore, O.G. Squalls, K.A. Waugh, E.B. Eruslanov, S. Singhal, J.D. Mitchell, W.A. Franklin, D.T. Merrick, et al. 2017. Antigen-Presenting Intratumoral B Cells Affect CD4$^+$ TIL Phenotypes in Non-Small Cell Lung Cancer Patients. *Cancer Immunol. Res*. 5:898–907. https://doi.org/10.1158/2326-6066.CIR-17-0075

Bukczynski, J., T. Wen, K. Ellefsen, J. Gauldie, and T.H. Watts. 2004. Costimulatory ligand 4-1BBL (CD137L) as an efficient adjuvant for human antiviral cytotoxic T cell responses. *Proc. Natl. Acad. Sci. USA*. 101:1291–1296. https://doi.org/10.1073/pnas.0306567101

Cabrita, R., M. Lauss, A. Sanna, M. Donia, M. Skaarup Larsen, S. Mitra, I. Johansson, B. Phung, K. Harbst, J. Vallon-Christersson, et al. 2020. Tertiary lymphoid structures improve immunotherapy and survival in melanoma. *Nature*. 577:561–565. https://doi.org/10.1038/s41586-019-1914-8

Chester, C., M.F. Sanmamed, J. Wang, and I. Melero. 2018. Immunotherapy targeting 4-1BB: mechanistic rationale, clinical results, and future strategies. *Blood*. 131:49–57. https://doi.org/10.1182/blood-2017-06-741041

Cyster, J.G., and C.C. Goodnow. 1995. Pertussis toxin inhibits migration of B and T lymphocytes into splenic white pulp cords. *J. Exp. Med*. 182:581–586. https://doi.org/10.1084/jem.182.2.581

DeRenzo, C., and S. Gottschalk. 2019. Genetic Modification Strategies to Enhance CAR T Cell Persistence for Patients With Solid Tumors. *Front. Immunol*. 10:218. https://doi.org/10.3389/fimmu.2019.00218

Eagles, M.E., F. Nassiri, J.H. Badhiwala, S. Suppiah, S.A. Almenawer, G. Zadeh, and K.D. Aldape. 2018. Dendritic cell vaccines for high-grade gliomas. *Ther. Clin. Risk Manag*. 14:1299–1313. https://doi.org/10.2147/TCRM.S135865

Ellsworth, S., A. Balmanoukian, F. Kos, C.J. Nirschl, T.R. Nirschl, S.A. Grossman, L. Luznik, and C.G. Drake. 2014. Sustained CD4$^+$ T cell-driven lymphopenia without a compensatory IL-7/IL-15 response among high-grade glioma patients treated with radiation and temozolomide. *OncoImmunology*. 3. e27357. https://doi.org/10.4161/onci.27357

Epeldegui, M., D.V. Conti, Y. Guo, W. Cozen, M.L. Penichet, and O. Martínez-Maza. 2019. Elevated numbers of PD-L1 expressing B cells are associated with the development of AIDS-NHL. *Sci. Rep*. 9:9371. https://doi.org/10.1038/s41598-019-45479-3

Freeman, G.J., A.J. Long, Y. Iwai, K. Bourque, T. Chernova, H. Nishimura, L.J. Fitz, N. Malenkovich, T. Okazaki, M.C. Byrne, et al. 2000. Engagement of the PD-1 immunoinhibitory receptor by a novel B7 family member leads to negative regulation of lymphocyte activation. *J. Exp. Med*. 192:1027–1034. https://doi.org/10.1084/jem.192.7.1027

Fu, C., and A. Jiang. 2018. Dendritic Cells and CD8 T Cell Immunity in Tumor Microenvironment. *Front. Immunol*. 9:3059. https://doi.org/10.3389/fimmu.2018.03059

Futagawa, T., H. Akiba, T. Kodama, K. Takeda, Y. Hosoda, H. Yagita, and K. Okumura. 2002. Expression and function of 4-1BB and 4-1BB ligand on murine dendritic cells. *Int. Immunol*. 14:275–286. https://doi.org/10.1093/intimm/14.3.275

Garaud, S., L. Buisseret, C. Solinas, C. Gu-Trantien, A. de Wind, G. Van den Eynden, C. Naveaux, J.N. Lodewyckx, A. Boisson, H. Duvillier, et al. 2019. Tumor infiltrating B-cells signal functional humoral immune responses in breast cancer. *JCI Insight*. 5. e129541.

Gonzalez, N.K., K. Wennhold, S. Balkow, E. Kondo, B. Bölck, T. Weber, M. Garcia-Marquez, S. Grabbe, W. Bloch, M. von Bergwelt-Baildon, et al. 2015. *In vitro* and *in vivo* imaging of initial B-T-cell interactions in the setting of B-cell based cancer immunotherapy. *OncoImmunology*. 4. e1038684. https://doi.org/10.1080/2162402X.2015.1038684

Goodwin, R.G., W.S. Din, T. Davis-Smith, D.M. Anderson, S.D. Gimpel, T.A. Sato, C.R. Maliszewski, C.I. Brannan, N.G. Copeland, N.A. Jenkins, et al. 1993. Molecular cloning of a ligand for the inducible T cell gene 4-1BB: a member of an emerging family of cytokines with homology to tumor necrosis factor. *Eur. J. Immunol*. 23:2631–2641. https://doi.org/10.1002/eji.1830231037

Grossman, S.A., X. Ye, G. Lesser, A. Sloan, H. Carraway, S. Desideri, and S. Piantadosi; NABTT CNS Consortium. 2011. Immunosuppression in patients with high-grade gliomas treated with radiation and temozolomide. *Clin. Cancer Res*. 17:5473–5480. https://doi.org/10.1158/1078-0432.CCR-11-0774

Grossman, S.A., S. Ellsworth, J. Campian, A.T. Wild, J.M. Herman, D. Laheru, M. Brock, A. Balmanoukian, and X. Ye. 2015. Survival in Patients With Severe Lymphopenia Following Treatment With Radiation and Chemotherapy for Newly Diagnosed Solid Tumors. *J. Natl. Compr. Canc. Netw.* 13:1225–1231. https://doi.org/10.6004/jnccn.2015.0151

Guan, H., Y. Wan, J. Lan, Q. Wang, Z. Wang, Y. Li, J. Zheng, X. Zhang, Z. Wang, Y. Shen, et al. 2016. PD-L1 is a critical mediator of regulatory B cells and T cells in invasive breast cancer. *Sci. Rep.* 6:35651. https://doi.org/10.1038/srep35651

Helmink, B.A., S.M. Reddy, J. Gao, S. Zhang, R. Basar, R. Thakur, K. Yizhak, M. Sade-Feldman, J. Blando, G. Han, et al. 2020. B cells and tertiary lymphoid structures promote immunotherapy response. *Nature.* 577:549–555. https://doi.org/10.1038/s41586-019-1922-8

Iranzo, J., I. Martincorena, and E.V. Koonin. 2018. Cancer-mutation network and the number and specificity of driver mutations. *Proc. Natl. Acad. Sci. USA.* 115:E6010–E6019. https://doi.org/10.1073/pnas.1803155115

Jourdan, M., N. Robert, M. Cren, C. Thibaut, C. Duperray, A. Kassambara, M. Cogné, K. Tarte, B. Klein, and J. Moreaux. 2017. Characterization of human FCRL4-positive B cells. *PLoS One.* 12. e0179793. https://doi.org/10.1371/journal.pone.0179793

Kim, E.K., H.S. Seo, M.J. Chae, I.S. Jeon, B.Y. Song, Y.J. Park, H.M. Ahn, C.O. Yun, and C.Y. Kang. 2014. Enhanced antitumor immunotherapeutic effect of B-cell-based vaccine transduced with modified adenoviral vector containing type 35 fiber structures. *Gene Ther.* 21:106–114. https://doi.org/10.1038/gt.2013.65

Lapointe, R., A. Bellemare-Pelletier, F. Housseau, J. Thibodeau, and P. Hwu. 2003. CD40-stimulated B lymphocytes pulsed with tumor antigens are effective antigen-presenting cells that can generate specific T cells. *Cancer Res.* 63:2836–2843.

Lee-Chang, C., M. Bodogai, K. Moritoh, P.B. Olkhanud, A.C. Chan, M. Croft, J.A. Mattison, P.J. Holst, R.E. Gress, L. Ferrucci, et al. 2014. Accumulation of 4-1BBL+ B cells in the elderly induces the generation of granzyme-B+ CD8+ T cells with potential antitumor activity. *Blood.* 124:1450–1459. https://doi.org/10.1182/blood-2014-03-563940

Lee-Chang, C., M. Bodogai, K. Moritoh, X. Chen, R. Wersto, R. Sen, H.A. Young, M. Croft, L. Ferrucci, and A. Biragyn. 2016. Aging Converts Innate B1a Cells into Potent CD8+ T Cell Inducers. *J. Immunol.* 196:3385–3397. https://doi.org/10.4049/jimmunol.1502034

Lee-Chang, C., A. Rashidi, J. Miska, P. Zhang, K.C. Pituch, D. Hou, T. Xiao, M. Fischietti, S.J. Kang, C.L. Appin, et al. 2019. Myeloid-Derived Suppressive Cells Promote B cell-Mediated Immunosuppression via Transfer of PD-L1 in Glioblastoma. *Cancer Immunol. Res.* 7:1928–1943. https://doi.org/10.1158/2326-6066.CIR-19-0240

Li, Z., S. Bao, Q. Wu, H. Wang, C. Eyler, S. Sathornsumetee, Q. Shi, Y. Cao, J. Lathia, R.E. McLendon, et al. 2009. Hypoxia-inducible factors regulate tumorigenic capacity of glioma stem cells. *Cancer Cell.* 15:501–513. https://doi.org/10.1016/j.ccr.2009.03.018

Louveau, A., J. Herz, M.N. Alme, A.F. Salvador, M.Q. Dong, K.E. Viar, S.G. Herod, J. Knopp, J.C. Setliff, A.L. Lupi, et al. 2018. CNS lymphatic drainage and neuroinflammation are regulated by meningeal lymphatic vasculature. *Nat. Neurosci.* 21:1380–1391. https://doi.org/10.1038/s41593-018-0227-9

Mackay, F., and J.L. Browning. 2002. BAFF: a fundamental survival factor for B cells. *Nat. Rev. Immunol.* 2:465–475. https://doi.org/10.1038/nri844

Mariño, E., B. Tan, L. Binge, C.R. Mackay, and S.T. Grey. 2012. B-cell cross-presentation of autologous antigen precipitates diabetes. *Diabetes.* 61:2893–2905. https://doi.org/10.2337/db12-0006

Maxwell, R., C.M. Jackson, and M. Lim. 2017. Clinical Trials Investigating Immune Checkpoint Blockade in Glioblastoma. *Curr. Treat. Options Oncol.* 18:51. https://doi.org/10.1007/s11864-017-0492-y

McCarron, M.J., P.W. Park, and D.R. Fooksman. 2017. CD138 mediates selection of mature plasma cells by regulating their survival. *Blood.* 129:2749–2759. https://doi.org/10.1182/blood-2017-01-761643

Melero, I., W.W. Shuford, S.A. Newby, A. Aruffo, J.A. Ledbetter, K.E. Hellström, R.S. Mittler, and L. Chen. 1997. Monoclonal antibodies against the 4-1BB T-cell activation molecule eradicate established tumors. *Nat. Med.* 3:682–685. https://doi.org/10.1038/nm0697-682

Mempel, T.R., S.E. Henrickson, and U.H. Von Andrian. 2004. T-cell priming by dendritic cells in lymph nodes occurs in three distinct phases. *Nature.* 427:154–159. https://doi.org/10.1038/nature02238

Miska, J., A. Rashidi, A.L. Chang, M.E. Muroski, Y. Han, L. Zhang, and M.S. Lesniak. 2016. Anti-GITR therapy promotes immunity against malignant glioma in a murine model. *Cancer Immunol. Immunother.* 65:1555–1567. https://doi.org/10.1007/s00262-016-1912-8

Nabors, L.B., J.G. Supko, M. Rosenfeld, M. Chamberlain, S. Phuphanich, T. Batchelor, S. Desideri, X. Ye, J. Wright, S. Gujar, et al; New Approaches to Brain Tumor Therapy (NABTT) CNS Consortium. 2011. Phase I trial of sorafenib in patients with recurrent or progressive malignant glioma. *Neuro-oncol.* 13:1324–1330. https://doi.org/10.1093/neuonc/nor145

Nielsen, J.S., R.A. Sahota, K. Milne, S.E. Kost, N.J. Nesslinger, P.H. Watson, and B.H. Nelson. 2012. CD20+ tumor-infiltrating lymphocytes have an atypical CD27- memory phenotype and together with CD8+ T cells promote favorable prognosis in ovarian cancer. *Clin. Cancer Res.* 18:3281–3292. https://doi.org/10.1158/1078-0432.CCR-12-0234

Petitprez, F., A. de Reyniès, E.Z. Keung, T.W. Chen, C.M. Sun, J. Calderaro, Y.M. Jeng, L.P. Hsiao, L. Lacroix, A. Bougoüin, et al. 2020. B cells are associated with survival and immunotherapy response in sarcoma. *Nature.* 577:556–560. https://doi.org/10.1038/s41586-019-1906-8

Pituch, K.C., J. Miska, G. Krenciute, W.K. Panek, G. Li, T. Rodriguez-Cruz, M. Wu, Y. Han, M.S. Lesniak, S. Gottschalk, et al. 2018. Adoptive Transfer of IL13Rα2-Specific Chimeric Antigen Receptor T Cells Creates a Pro-inflammatory Environment in Glioblastoma. *Mol. Ther.* 26:986–995. https://doi.org/10.1016/j.ymthe.2018.02.001

Prins, R.M., X. Wang, H. Soto, E. Young, D.N. Lisiero, B. Fong, R. Everson, W.H. Yong, A. Lai, G. Li, et al. 2013. Comparison of glioma-associated antigen peptide-loaded versus autologous tumor lysate-loaded dendritic cell vaccination in malignant glioma patients. *J. Immunother.* 36:152–157. https://doi.org/10.1097/CJI.0b013e3182811ae4

Raychaudhuri, B., P. Rayman, J. Ireland, J. Ko, B. Rini, E.C. Borden, J. Garcia, M.A. Vogelbaum, and J. Finke. 2011. Myeloid-derived suppressor cell accumulation and function in patients with newly diagnosed glioblastoma. *Neuro-oncol.* 13:591–599. https://doi.org/10.1093/neuonc/nor042

Sanchez-Perez, L., B.D. Choi, E.A. Reap, E.J. Sayour, P. Norberg, R.J. Schmittling, G.E. Archer, J.E. Herndon, II, D.A. Mitchell, A.B. Heimberger, et al. 2013. BLyS levels correlate with vaccine-induced antibody titers in patients with glioblastoma lymphodepleted by therapeutic temozolomide. *Cancer Immunol. Immunother.* 62:983–987. https://doi.org/10.1007/s00262-013-1405-y

Saraswathula, A., E.A. Reap, B.D. Choi, R.J. Schmittling, P.K. Norberg, E.J. Sayour, J.E. Herndon, II, P. Healy, K.L. Congdon, G.E. Archer, et al. 2016. Serum elevation of B lymphocyte stimulator does not increase regulatory B cells in glioblastoma patients undergoing immunotherapy. *Cancer Immunol. Immunother.* 65:205–211. https://doi.org/10.1007/s00262-015-1784-3

Schultze, J.L., S. Michalak, M.J. Seamon, G. Dranoff, K. Jung, J. Daley, J.C. Delgado, J.G. Gribben, and L.M. Nadler. 1997. CD40-activated human B cells: an alternative source of highly efficient antigen presenting cells to generate autologous antigen-specific T cells for adoptive immunotherapy. *J. Clin. Invest.* 100:2757–2765. https://doi.org/10.1172/JCI119822

Sims, J.S., B. Grinshpun, Y. Feng, T.H. Ung, J.A. Neira, J.L. Samanamud, P. Canoll, Y. Shen, P.A. Sims, and J.N. Bruce. 2016. Diversity and divergence of the glioma-infiltrating T-cell receptor repertoire. *Proc. Natl. Acad. Sci. USA.* 113:E3529–E3537. https://doi.org/10.1073/pnas.1601012113

Stupp, R., S. Taillibert, A. Kanner, W. Read, D. Steinberg, B. Lhermitte, S. Toms, A. Idbaih, M.S. Ahluwalia, K. Fink, et al. 2017. Effect of Tumor-Treating Fields Plus Maintenance Temozolomide vs Maintenance Temozolomide Alone on Survival in Patients With Glioblastoma: A Randomized Clinical Trial. *JAMA.* 318:2306–2316. https://doi.org/10.1001/jama.2017.18718

Taphoorn, M.J.B., L. Dirven, A.A. Kanner, G. Lavy-Shahaf, U. Weinberg, S. Taillibert, S.A. Toms, J. Honnorat, T.C. Chen, J. Sroubek, et al. 2018. Influence of Treatment With Tumor-Treating Fields on Health-Related Quality of Life of Patients With Newly Diagnosed Glioblastoma: A Secondary Analysis of a Randomized Clinical Trial. *JAMA Oncol.* 4:495–504. https://doi.org/10.1001/jamaoncol.2017.5082

Thorsson, V., D.L. Gibbs, S.D. Brown, D. Wolf, T.H. Ou Yang, E. Porta-Pardo, G.F. Gao, C.L. Plaisier, J.A. Eddy, et al, N. Cancer Genome Atlas Research. 2018. The Immune Landscape of Cancer. *Immunity.* 48:812–830.e14.

Tsou, P., H. Katayama, E.J. Ostrin, and S.M. Hanash. 2016. The Emerging Role of B Cells in Tumor Immunity. *Cancer Res.* 76:5597–5601. https://doi.org/10.1158/0008-5472.CAN-16-0431

Uno, T., K. Takeda, Y. Kojima, H. Yoshizawa, H. Akiba, R.S. Mittler, F. Gejyo, K. Okumura, H. Yagita, and M.J. Smyth. 2006. Eradication of established tumors in mice by a combination antibody-based therapy. *Nat. Med.* 12:693–698. https://doi.org/10.1038/nm1405

Vega, E.A., M.W. Graner, and J.H. Sampson. 2008. Combating immunosuppression in glioma. *Future Oncol.* 4:433–442. https://doi.org/10.2217/14796694.4.3.433

Vinay, D.S., and B.S. Kwon. 1998. Role of 4-1BB in immune responses. *Semin. Immunol.* 10:481–489. https://doi.org/10.1006/smim.1998.0157

Wainwright, D.A., I.V. Balyasnikova, A.L. Chang, A.U. Ahmed, K.S. Moon, B. Auffinger, A.L. Tobias, Y. Han, and M.S. Lesniak. 2012a. IDO expression in brain tumors increases the recruitment of regulatory T cells and negatively impacts survival. *Clin. Cancer Res.* 18:6110–6121. https://doi.org/10.1158/1078-0432.CCR-12-2130

Wainwright, D.A., P. Nigam, B. Thaci, M. Dey, and M.S. Lesniak. 2012b. Recent developments on immunotherapy for brain cancer. *Expert Opin. Emerg. Drugs.* 17:181–202. https://doi.org/10.1517/14728214.2012.679929

Weller, M., N. Butowski, D.D. Tran, L.D. Recht, M. Lim, H. Hirte, L. Ashby, L. Mechtler, S.A. Goldlust, F. Iwamoto, et al; ACT IV trial investigators. 2017. Rindopepimut with temozolomide for patients with newly diagnosed, EGFRvIII-expressing glioblastoma (ACT IV): a randomised, double-blind, international phase 3 trial. *Lancet Oncol.* 18:1373–1385. https://doi.org/10.1016/S1470-2045(17)30517-X

Wen, P.Y., D.A. Reardon, T.S. Armstrong, S. Phuphanich, R.D. Aiken, J.C. Landolfi, W.T. Curry, J.J. Zhu, M. Glantz, D.M. Peereboom, et al. 2019. A Randomized Double-Blind Placebo-Controlled Phase II Trial of Dendritic Cell Vaccine ICT-107 in Newly Diagnosed Patients with Glioblastoma. *Clin. Cancer Res.* 25:5799–5807. https://doi.org/10.1158/1078-0432.CCR-19-0261

Wennhold, K., M. Thelen, H.A. Schlößer, N. Haustein, S. Reuter, M. Garcia-Marquez, A. Lechner, S. Kobold, F. Rataj, O. Utermöhlen, et al. 2017. Using Antigen-Specific B Cells to Combine Antibody and T Cell-Based Cancer Immunotherapy. *Cancer Immunol. Res.* 5:730–743. https://doi.org/10.1158/2326-6066.CIR-16-0236

Wennhold, K., A. Shimabukuro-Vornhagen, and M. von Bergwelt-Baildon. 2019. B Cell-Based Cancer Immunotherapy. *Transfus. Med. Hemother.* 46: 36–46. https://doi.org/10.1159/000496166

Wilson, E.H., W. Weninger, and C.A. Hunter. 2010. Trafficking of immune cells in the central nervous system. *J. Clin. Invest.* 120:1368–1379. https://doi.org/10.1172/JCI41911

Wintterle, S., B. Schreiner, M. Mitsdoerffer, D. Schneider, L. Chen, R. Meyermann, M. Weller, and H. Wiendl. 2003. Expression of the B7-related molecule B7-H1 by glioma cells: a potential mechanism of immune paralysis. *Cancer Res.* 63:7462–7467.

Yoshizaki, A., T. Miyagaki, D.J. DiLillo, T. Matsushita, M. Horikawa, E.I. Kountikov, R. Spolski, J.C. Poe, W.J. Leonard, and T.F. Tedder. 2012. Regulatory B cells control T-cell autoimmunity through IL-21-dependent cognate interactions. *Nature.* 491:264–268. https://doi.org/10.1038/nature11501

Zhang, P., J. Miska, C. Lee-Chang, A. Rashidi, W.K. Panek, S. An, M. Zannikou, A. Lopez-Rosas, Y. Han, T. Xiao, et al. 2019. Therapeutic targeting of tumor-associated myeloid cells synergizes with radiation therapy for glioblastoma. *Proc. Natl. Acad. Sci. USA.* 116:23714–23723. https://doi.org/10.1073/pnas.1906346116
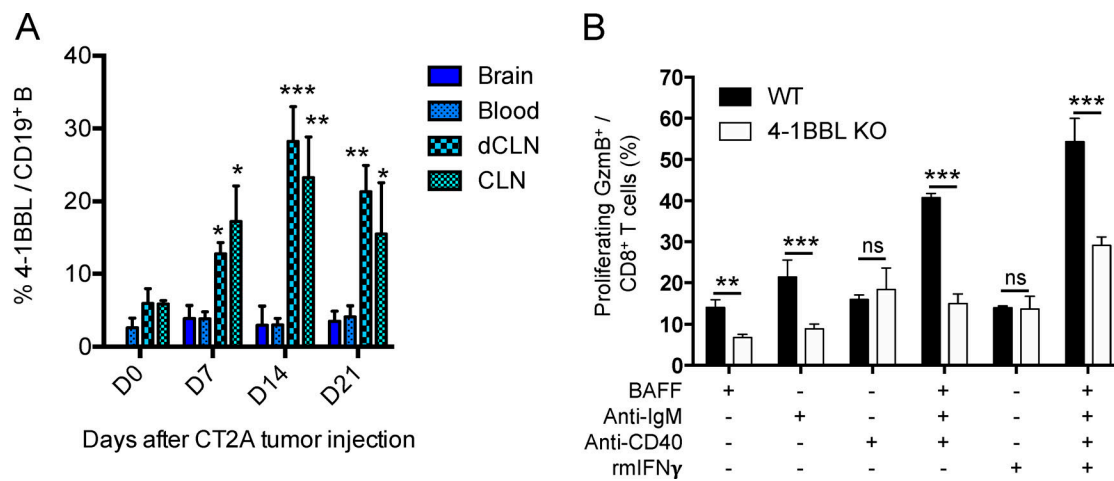
Figure S1. **4-1BBL–expressing B cells. (A)** 4-1BBL expression levels by CD19+ B cells in the brain, blood, dCLNs, and superficial CLNs of CT2A glioma-bearing mice over time: no tumor (D0), 7, 14, and 21 d after tumor implantation (n = 4 mice/time point). **(B)** Murine B cell ability to promote CD8+ T cell activation, measured by cell expansion and expression of intracellular GzmB, was assessed by activated B cells and compared with B cells from 4-1BBL–deficient (4-1BBL KO) mice. B cells were incubated with BAFF, anti-IgM, anti-CD40, and/or recombinant mouse (rm)IFNγ. Representative experiment of a total of three independent experiments performed in triplicate. Differences among multiple groups were evaluated using one-way ANOVA with post hoc Tukey's multiple comparisons test. Histograms are shown as mean ± SD. Statistical significance is depicted as follows: *, $P < 0.05$; **, $P < 0.01$; ***, $P < 0.001$. ns, not statistically significant.
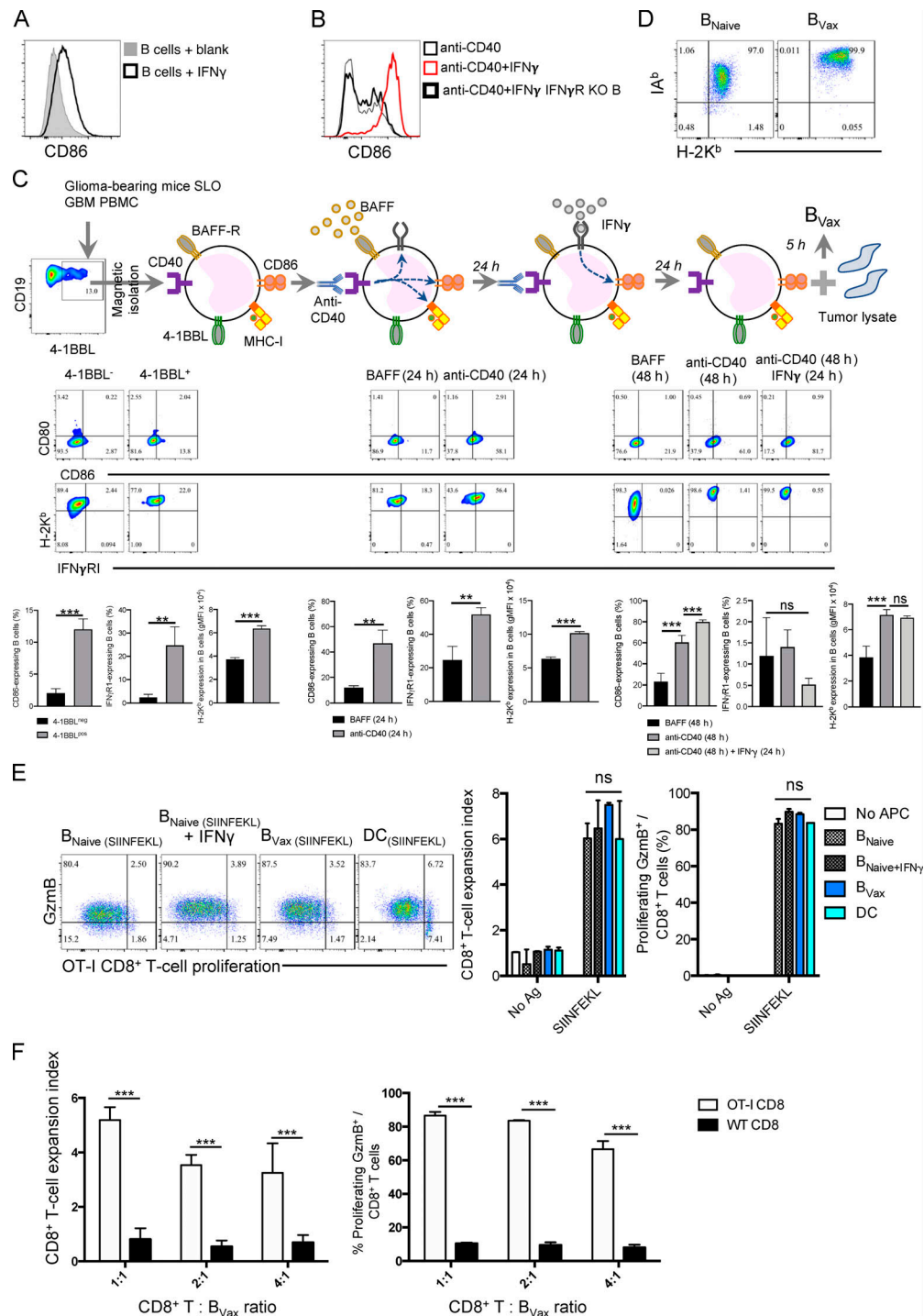
Figure S2. B_Vax generation. (A) Human B cells from PBMCs were treated with 10 U/ml IFNγ for 24 h. CD86 expression was assessed by flow cytometry. Representative histogram of three independent experiments. **(B)** Murine B cells from WT C57BL/6 or IFNγR–deficient (IFNγR KO) mice were incubated with 5 µg/ml CD40 activating Ab ± 10 U/ml IFNγ. Expression of CD86 was assessed by flow cytometry. Representative histogram of four independent experiments. **(C)** Stepwise schema of B_Vax generation in vitro. B_Vax were produced from 4-1BBL⁺ B cells isolated from tumor-bearing SLOs such as the spleen and deep and superficial CLNs. Cells were then activated with 5 µg/ml CD40 activating Ab and supplemented with 100 nM of B cell survival factor BAFF, which after 24 h allows the up-regulation of CD86, H-2K^b, and IFNγ receptor 1 (IFNγRI) compared with only BAFF-treated B cells. The addition of IFNγ for an additional 24 h allowed further up-regulation of CD86 compared with only anti-CD40–treated B cells. Histograms represent mean ± SD of n = 3 mice/treatment. gMFI, geometric mean fluorescence intensity. **(D)** B_Vax overexpress both IA^b (MHC class II) and H-2K^b compared with only BAFF-treated B cells (B_Naive). Flow cytometry dot plot representative of n = 4 mice/group. **(E)** B cell subsets (B_Naive ± IFNγ and B_Vax) and DCs were tested for their ability to present SIINFEKL peptide to OT-I CD8⁺ T cells measured by cell proliferation and expression of intracellular GzmB. Representative experiment of three independent experiments performed in triplicate. **(F)** Same experiment as in E was performed using in addition CD8⁺ T cells from WT C57BL/6 mice as negative control. Differences among multiple groups were evaluated using one-way ANOVA with post hoc Tukey's multiple comparisons test. Histograms are shown as mean ± SD. Statistical significance is depicted as follows: *, $P < 0.05$; **, $P < 0.01$; ***, $P < 0.001$. ns, not statistically significant.
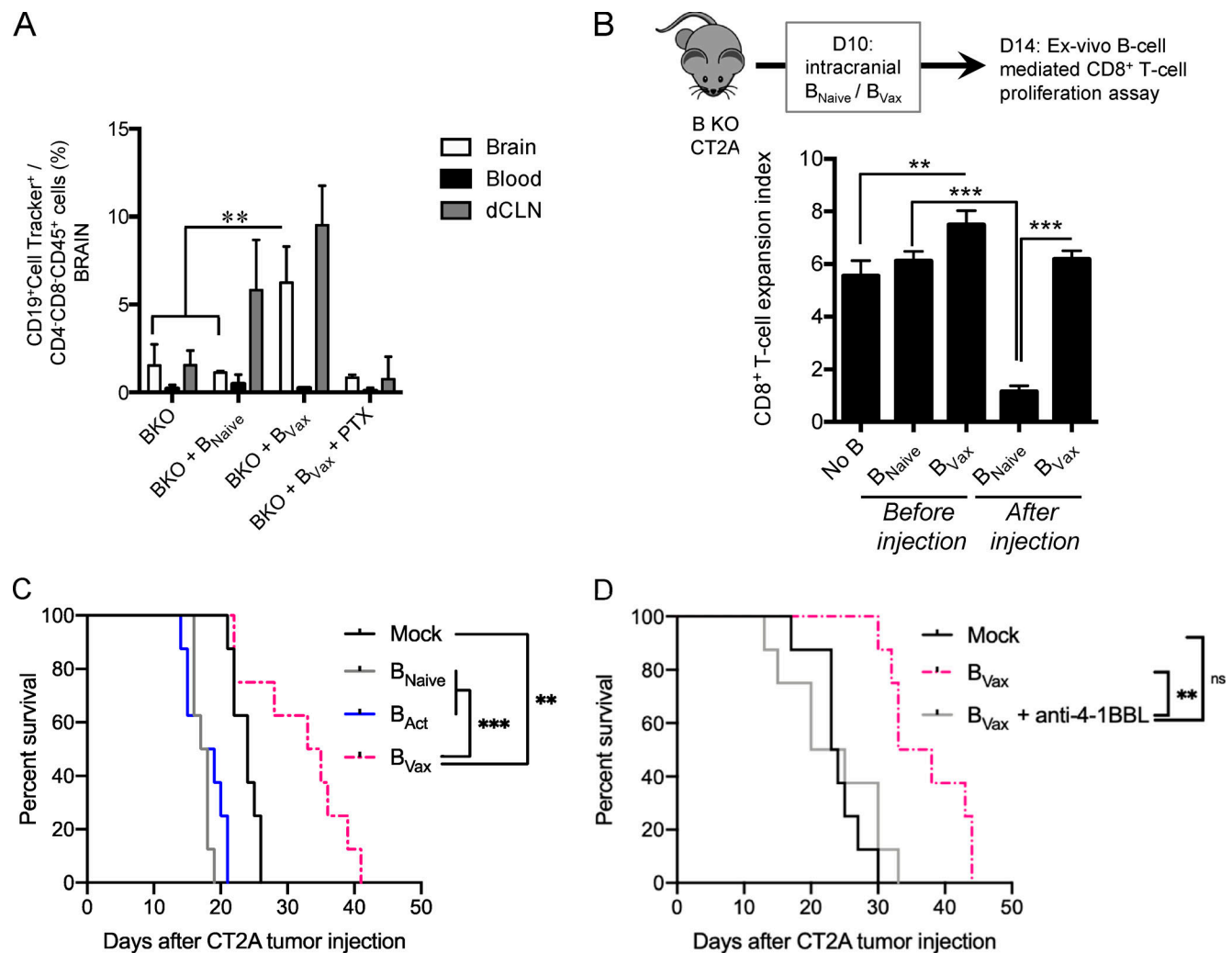
Figure S3.   **4-1BBL is a key marker for B$_{Vax}$ therapeutic effect. (A)** In B cell–deficient mice, B$_{Naive}$ and B$_{Vax}$ were detected in draining dCLNs and the circulation, and B$_{Vax}$ were found in the tumor-bearing brains. Histogram represents mean ± SD of n = 5 mice/group. **(B)** CD45.1$^+$ B$_{Naive}$ and B$_{Vax}$ were intracranially injected using cannula-guided injections 10 d after tumor implantation. 4 d after, CD45.1$^+$ cells were magnetically isolated from tumors and tested for their ability to activate CD8$^+$ T cells, measured by cell proliferation (expansion index) by flow cytometry. Histogram represents mean ± SD of n = 3 mice/group. **(C)** B$_{Naive}$, B$_{Act}$, and B$_{Vax}$ were tested for their therapeutic effect in CT2A-bearing B cell–deficient (B KO) mice (n = 9 or 10 mice/group). **(D)** CT2A-bearing B cell–deficient mice treated with B$_{Vax}$ (pretreated with 4-1BBL–blocking Ab before injection) ± 4-1BBL–blocking Ab (500 µg/mouse × three i.p. injections after B$_{Vax}$ adoptive transfer) were monitored for survival (n = 10 mice/group). Differences among multiple groups were evaluated using one-way ANOVA with post hoc Tukey's multiple comparisons test. Survival curves were generated via the Kaplan-Meier method and compared by log-rank test, and multiple comparisons were adjusted using Bonferroni method. Statistical significance is depicted as follows: *, P < 0.05; **, P < 0.01; ***, P < 0.001. ns, not statistically significant.
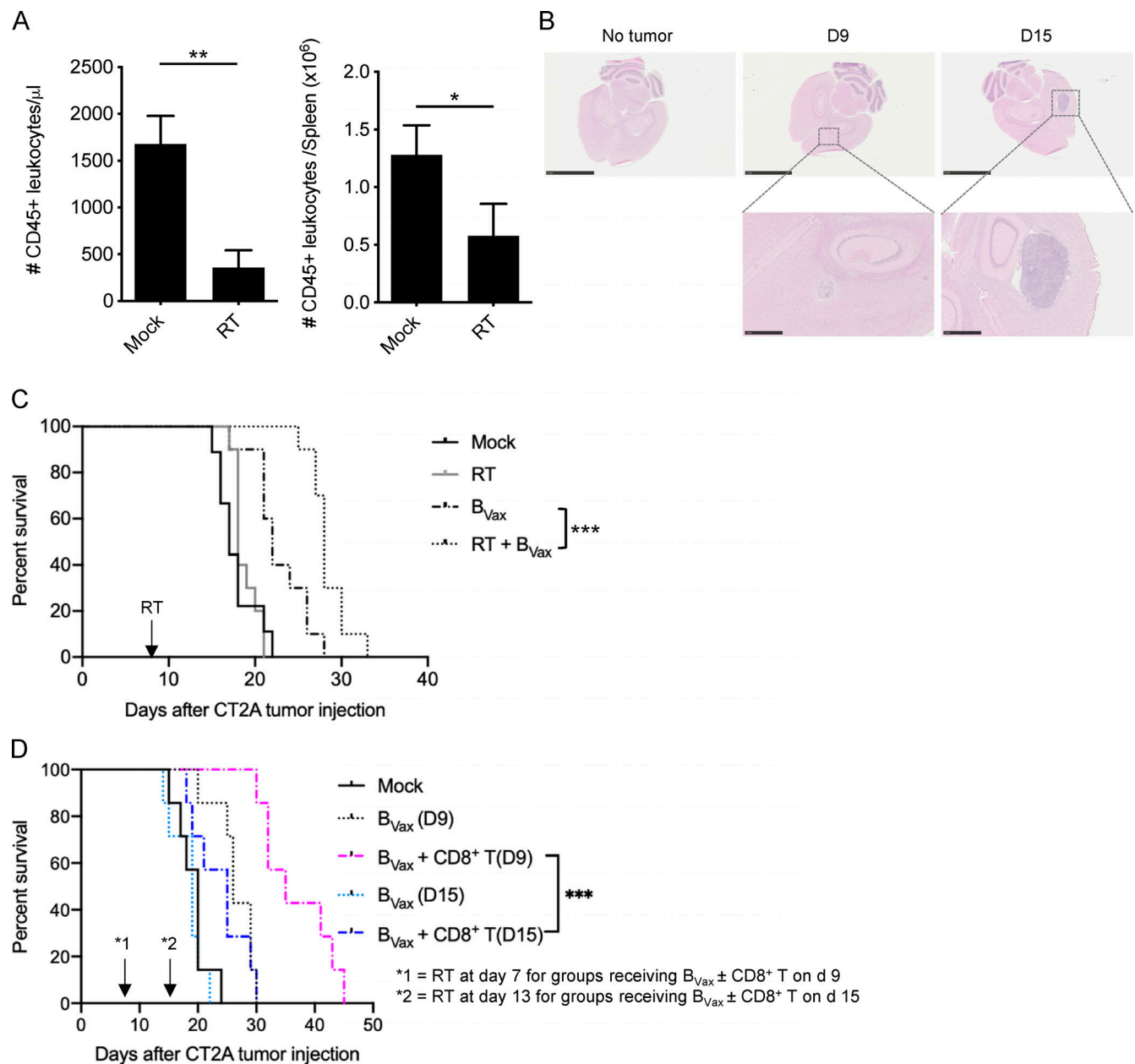
Figure S4. **B_Vax therapeutic effect. (A)** RT-induced systemic leukopenia measured by CD45+ leukocytes in blood and in the spleen (n = 4 mice/group). **(B)** Histological evaluation of CT2A tumor burden at different time points (9 [D9] and 15 d [D15] after tumor implantation). All mice received 9-Gy radiation 7 d after tumor inoculation. **(C)** B_Vax therapeutic effect was evaluated in animals that received RTx 7 d after tumor implantation and/or B_Vax treatment 9 d after tumor implantation (n = 10 mice/group). **(D)** B_Vax + CD8+ T cell treatment efficacy was tested at different time points: 9 and 15 d after tumor inoculation. All mice received RTx 7 d after tumor injection (n = 7 mice/group). Differences between the two groups were analyzed by Student's t test. Histograms are shown as mean ± SD. Survival curves were generated via the Kaplan-Meier method and compared by log-rank test and multiple comparisons were adjusted using the Bonferroni method. Statistical significance is depicted as *, $P < 0.05$; **, $P < 0.01$; ***, $P < 0.001$. ns, not statistically significant.
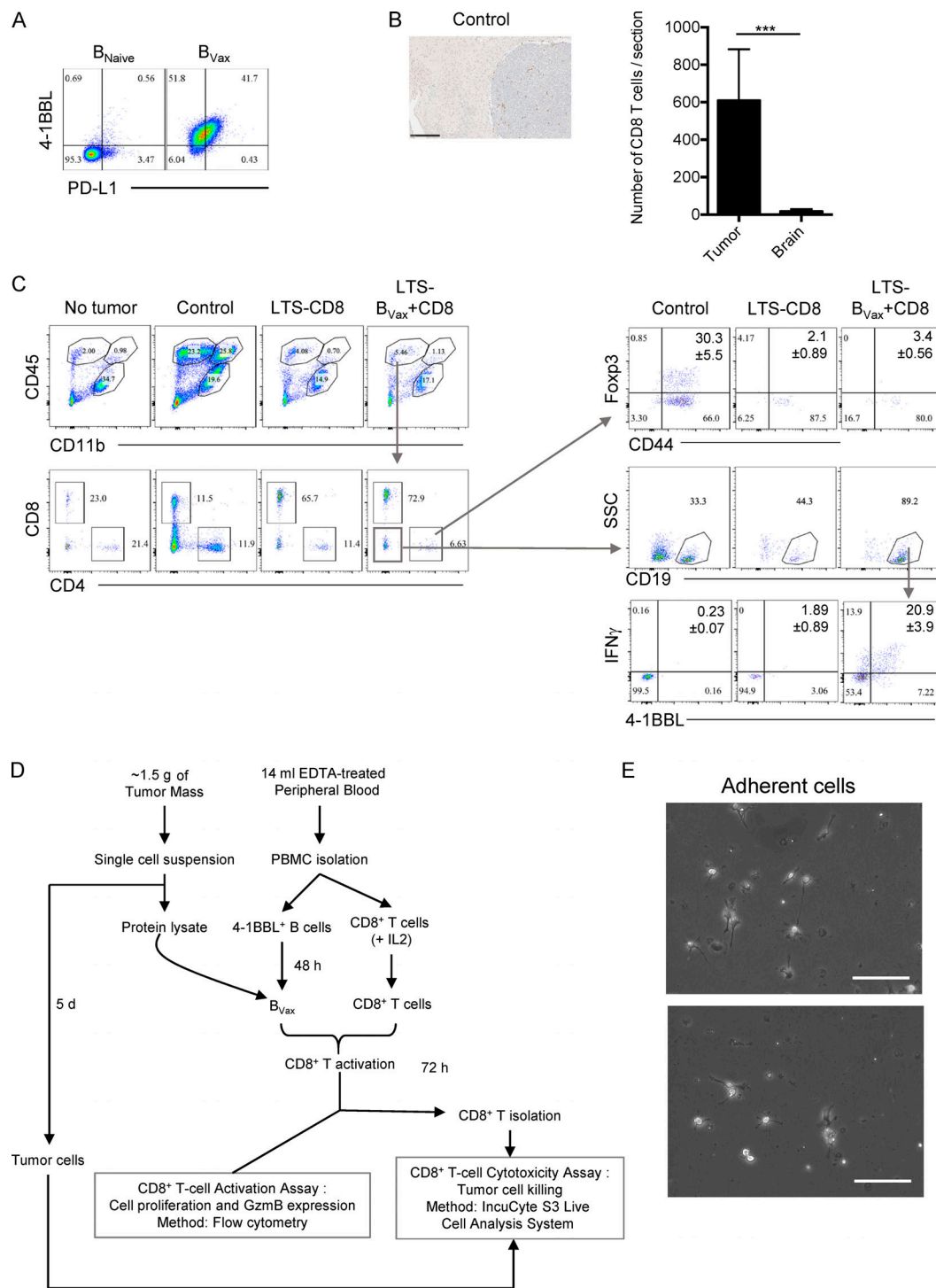
Figure S5. **B$_{Vax}$ treatment confers tumor eradication. (A)** PD-L1 membrane expression was evaluated in B$_{Vax}$ and B$_{Naive}$ cells. Representative dot plot of four independent experiments. Histograms are shown as mean ± SD. **(B)** CD8$^+$ T cell infiltration in CT2A tumor in control group (14 d after tumor inoculation, $n = 2$). Scale bar represents 250 µm. Number of CD8$^+$ T cells per section was assessed in the tumor area (tumor) versus nontumor (brain) area. **(C)** Immune cell infiltration in LTSs treated with either B$_{Vax}$ and CD8$^+$ T cells (LTS-B$_{Vax}$+CD8, $n = 5$) or only CD8$^+$ T cells (LTS-CD8, $n = 4$) were compared with control CT2A-bearing (Control, $n = 3$) and Mock brains (No tumor, $n = 2$). Representative dot plot showing lymphocyte and myeloid cell compartment distribution (CD45 and CD11b expression) and CD8$^+$ and CD4$^+$ T cell distribution. Within the CD4$^+$ T cell compartment, the expression of CD44 and Foxp3 was evaluated. Within the non–T cell compartment (CD8$^-$CD4$^-$ lymphocytes), the CD19$^+$ B cell compartment–expressing IFNγ and 4-1BBL was evaluated. Values of the populations of interest are shown as mean ± SD. Differences between two groups were analyzed by Student's *t* test. Differences among multiple groups were evaluated using one-way ANOVA with post hoc Tukey's multiple comparisons test. GBM patient–derived B$_{Vax}$ promoted anti-tumor CD8$^+$ T cells. **(D)** Schema of generation of GBM patient–derived B$_{Vax}$. CD8$^+$ T cell activation and expansion and CD8$^+$ T cell–mediated tumor cell killing assay was performed in autologous settings. **(E)** Freshly resected tumors from GBM patients were cultured ex vivo as tumor spheroids. Representative picture of adherent cells after 5 d of culture. Scale bars represent 100 µm. SSC, side scatter.